New ionic mesogens with high ionic conductivity based on a cyanoborate building block and lipophilic or hydrophilic counter ions

Matthias Lehmann,*[a,b] Pascal Weinberger,[a] Maik Finze,[c] Guinevere A. Giffin,[d,e] Mario Weller,[e] Stephanie Bachmann[a] and Ann-Christin Pöppler[a]

[a]*Institute of Organic Chemistry, University of Würzburg, Am Hubland, 97074 Würzburg, Germany*
E-mail: matthias.lehmann@uni-wuerzburg.de

[b]*Center for Nanosystems Chemistry and Bavarian Polymer Institute, University of Würzburg, Am Hubland, 97074 Würzburg, Germany*

[c]*Institute of Inorganic Chemistry and Institute for Sustainable Chemistry & Catalysis with Boron - ICB, University of Würzburg, Am Hubland, 97074 Würzburg, Germany*

[d]*Fraunhofer Institute for Silicate Research, Neunerplatz 2, 97082 Würzburg, Germany*

[e]*Chemical Technology of Materials Synthesis, Faculty of Chemistry and Pharmacy, Julius-Maximilians-University Würzburg, Roentgenring 11, 97070 Würzburg, Germany*

Supporting Information

Contents

1) General Information

All commercial materials employed were used as received without further purification. ^{1}H- ^{13}C- and ^{11}B NMR spectra were recorded on a Bruker-Daltonics *Avance-400* spectrometer operating at 401 MHz (^{1}H), 101 MHz (^{13}C) or 128 MHz (^{11}B). NMR signals were referenced against TMS (^{1}H and ^{13}C) and $BF_3{\cdot}OEt_2$ (^{11}B), while the residual solvent signals were used as the internal standard. The information for NMR characterization of new compounds and the assignment of ^{1}H- ^{13}C- and ^{11}B atom signals was drawn from ^{1}H, ^{13}C, ^{11}B, DEPT135, COSY, HSQC and HMBC standard measurement methods. Mass spectra were recorded on a Bruker-Daltonics *autflex II* (MALDI) and on a Bruker-Daltonics *ultrafleXtreme* (HRMS-MALDI). FT-IR spectra were recorded with a JASCO *FT/IR-4600*. The samples were prepared as thin films.

The studies of optical textures of the mesophases were realized with a Nikon *Eclipse LV100Pol* optical polarizing microscope equipped with a Linkam *LTS420* heating stage, a Linkam *T95-HS* system controller and a StellarNet *BLACK-Comet CXR-100* USB Spectrometer. The temperature dependent SAXS, MAXS and WAXS X-ray investigations were performed on a Bruker Nanostar (Detector Vantec2000, Microfocus copper anode X-ray tube Incoatec). The aligned fibers were transferred to Mark capillaries, which were sealed and glued into the metal sample holder. The XRS heating system was calibrated by liquid crystal standard compounds. The XRS data was evaluated by the program Datasqueeze[S1] using silver behenate as a calibration standard.

Experimental studies on alignment in LC cells were made in ITO glass cells (Instec, Inc.) with sandwich electrodes. AxioImager D1 polarizing microscope (Carl Zeiss GmbH) were used equipped with the hot stage TS200 (Linkam). The measurements were made in orthoscopic and conoscopic setting. Optical observations have been performed using 8 μm glass cells with ITO electrodes. The material was introduced into the cells using capillary suction in its isotropic state.

2) Synthesis

Synthetic scheme for synthesis of hydroxyalkyl dodecyloxybenzoates and tricyano(benzoyloxyalkoxy)carbonylborates

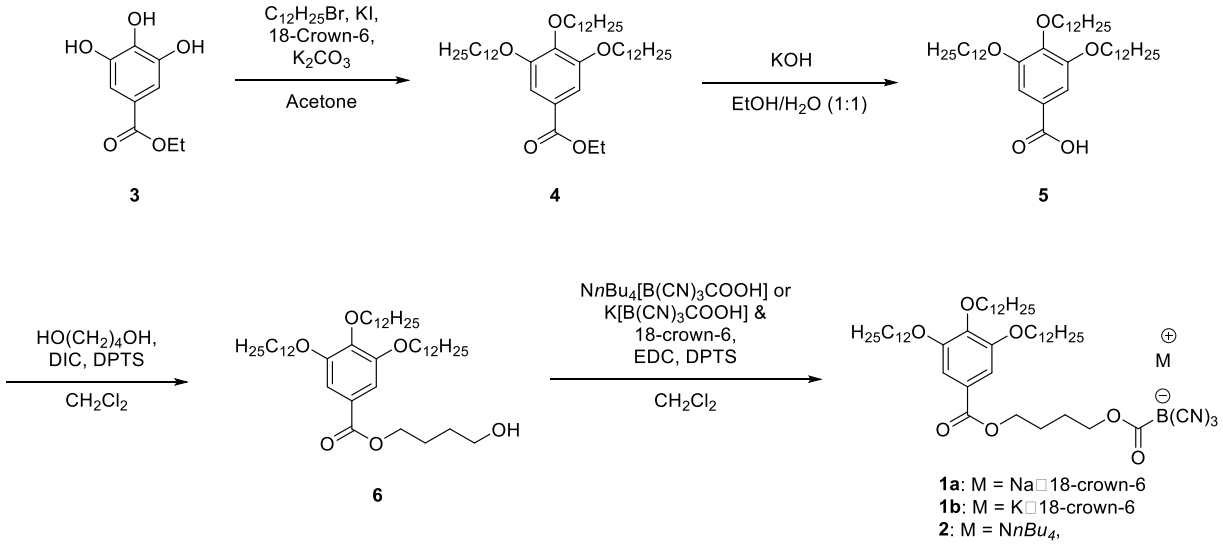

Scheme S1. Synthesis of molecules **1a**, **1b** and **2**. DIC = *N*,*N*′-Diisopropylcarbodiimid, DPTS = 4-(Dimethylamino)pyridinium 4-toluene-sulfonate, EDC = 1-Ethyl-3-(3-dimethylaminopropyl)carbodiimid

Synthesis of methyl 3,4,5-tris(dodecyloxy)benzoate (**4**)

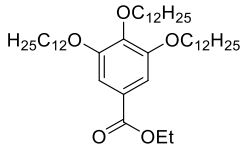

Compound **4** was synthesized according to a modified literature procedure.[S2] Ethyl 3,4,5-trihydroxybenzoate (5.00 g, 25.2 mmol), potassium iodide (377 mg, 2.27 mmol) and 18-crown-6 (200 mg, 757 µmol) were dissolved in acetone (250 mL). Under vigorous stirring, potassium carbonate (34.9 g, 252 mmol) as well as 1-bromododecane (24.2 mL, 25.2 g, 101 mmol) were added. The suspension was heated to reflux and stirred for 72 h. After cooling to room temperature (RT), the remaining solid was filtered and washed with acetone. The filtered solution was concentrated and dichloromethane (DCM) (100 mL) was added. The organic layer was washed with water and dried over Na_2SO_4. The solvent was removed under reduced pressure. The crude product was purified by column chromatography (SiO_2,

cyclohexane / DCM = 1 : 0 → 2 : 1 → 1 : 1, *v* / *v* → EA) to yield **4** as an off-white solid (13.5 g, 76%). ^{1}H NMR (401 MHz, $CDCl_3$, Me_4Si): δ = 0.88 (t, ^3J = 6.9 Hz, 9 H, $O(CH)_{11}CH_3$), 1.22–1.38 (m, 48 H, $O(CH_2)_3(CH_2)_8CH_3$), 1.38 (t, ^3J = 7.1 Hz, 3 H, $CO_2CH_2CH_3$), 1.43–1.51 (m, 6 H, $O(CH_2)_2CH_2(CH_2)_8CH_3$), 1.70–1.85 (m, 6 H, $OCH_2CH_2(CH_2)_9CH_3$), 4.01 (t, ^3J = 6.5 Hz, 6 H, $OCH_2CH_2(CH_2)_9CH_3$), 4.35 (q, ^3J = 7.1 Hz, 3 H, $CO_2CH_2CH_3$), 7.25 (s, 2 H, aromat. H) ppm.

Synthesis of 3,4,5-tris(dodecyloxy)benzoic acid (**5**)

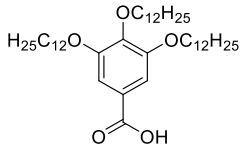

Compound **5** was synthesized according to a modified literature procedure.[S3] Compound **4** (6.00 g, 8.53 mmol) was dissolved in a ethanol (EtOH) / H_2O (200 mL, 1 : 1, *v* / *v*) mixture and potassium hydroxide(19.0 g, 339 mmol) was added. The mixture was heated to reflux for 16 h. After cooling to RT, EtOH was removed under reduced pressure and the residue was acidified using 1 M aqueous HCl. The aqueous phase was extracted with DCM and the organic phases were dried over Na_2SO_4. The solvent was removed under reduced pressure. The crude product was recrystallized from EtOH to yield **5** as white crystals (5.45 g, 95%). ^{1}H NMR (401 MHz, $CDCl_3$, Me_4Si): δ = 0.88 (t, ^3J = 6.9 Hz, 9 H, $O(CH)_{11}CH_3$), 1.22–1.38 (m, 48 H, $O(CH_2)_3(CH_2)_8CH_3$), 1.43–1.51 (m, 6 H, $O(CH_2)_2CH_2(CH_2)_8CH_3$), 1.71–1.86 (m, 6 H, $OCH_2CH_2(CH_2)_9CH_3$), 4.02 (t, ^3J = 6.6 Hz, 4 H, *m*-$OCH_2CH_2(CH_2)_9CH_3$), 4.04 (t, ^3J = 6.6 Hz, 2 H, *p*-$OCH_2CH_2(CH_2)_9CH_3$), 7.30 (s, 2 H, aromat. H) ppm.

Synthesis of 4-hydroxybutyl 3,4,5-tris(dodecyloxy)benzoate (**6**)

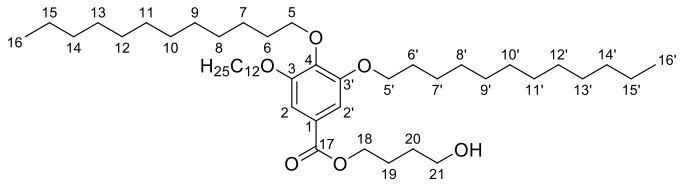

Compound **6** was synthesized according to a modified literature procedure.[S4] Under nitrogen atmosphere a solution of compound **5** (1.00 g, 1.48 mmol) and 1,4-butanediol (160 µL,160 mg, 1.8 µmol) in dry DCM (2 mL) was slowly added to a solution of DPTS (654 mg, 2.22 mmol) and DIC (460 µL, 370 mg, 2.9 mmol) in dry DCM (2 mL). The solution was stirred at RT for 16 h. The reaction mixture was washed with 25 mL of 1 M aqueous HCl and the aqueous phase was extracted with DCM. The organic phase was dried over Na_2SO_4 and the solvent was removed under reduced pressure. The crude product was purified by column chromatography (SiO_2, cyclohexane / EA = 3 : 1, *v* / *v*) to yield **6** as an off-white solid (1.00 g, 91%). Mp: 40.3 °C. ^{1}H NMR (401 MHz, $CDCl_3$, Me_4Si): δ = 0.88 (t, ^3J = 6.9 Hz, 9 H, H-16/16'), 1.22–1.38 (m, 48 H, H-8–15/8'–15'), 1.43–1.50 (m, 6 H, H-7/7'), 1.68–1.75 (m, 2 H, H-6), 1.77–1.85 (m, 4 H, H-6'), 1.85–1.90 (m, 2 H, H-19), 3.73 (t, ^3J = 6.4 Hz, 2 H, H-21), 4.00 (t, ^3J = 6.5 Hz, 4 H, H-5'), 4.01 (t, ^3J = 6.5 Hz, 2 H, H-5), 4.34 (t, ^3J = 6.6 Hz, 2 H, H-18), 7.24 (s, 2 H, H-2/2') ppm. ^{13}C NMR (101 MHz, $CDCl_3$, Me_4Si): δ = 14.3 (C_p, C-16/16'), 22.9 (C_s, C-8–15/8'–15'), 25.4 (C_s, C-19), 26.2(0) (C_s, C-7), 26.2(4) (C_s, C-7'), 29.3 (C_s, C-20), 29.4(6) (C_s, C-6'), 29.5(2), 29.5(5), 29.7(2), 29.7(9), 29.8(1), 29.8(5), 29.8(8), 29.8(9), 29.9 (C_s, C-8–15/8'–15'), 30.5 (C_s, C-6), 32.0(8), 32.0(9) (C_s, C-8–15/8'–15'), 62.6 (C_s, C-21), 64.9 (C_s, C-18), 69.3 (C_s, C-5), 73.7 (C_s, C-5'), 108.1 (C_t, H-2), 125.0 (C_q, C-1), 142.5 (C_q, C-4), 153.0 (C_q, C, C-3/3'), 166.7 (C_q, C-17) ppm. HRMS (MALDI) *m*/*z*: [$C_{47}H_{86}NaO_7$] Calcd for $C_{47}H_{86}NaO_7$ 769.6322 (Chemdraw), .769.6317 (MALDI); Found 769.62941.

Tetrabutylammonium tricyano({4-[3,4,5-tris(dodecyloxy)benzoyloxy]butoxy}carbonyl)borate (**2**)

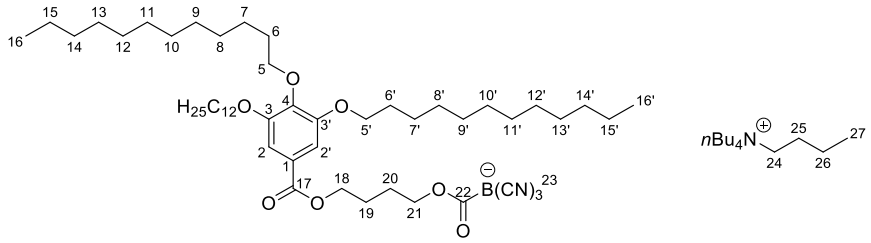

ILC **2** was synthesized according to a modified literature procedure.[S4] Under nitrogen atmosphere, a solution of **6** (102 mg, 136 µmol) and nBu$_4$N[B(CN)$_3$CO$_2$H] (90.0 mg, 238 µmol) in dry DCM (2 mL) was slowly added to a solution of DPTS (120 mg, 408 µmol) and EDC (100 µL, 90 mg, 580 µmol) in dry DCM (2 mL). The solution was stirred at RT for 16 h. The reaction mixture was washed with 25 mL of 1 M aqueous HCl and the aqueous phase was extracted with DCM. The organic phase was dried over Na_2SO_4 and the solvent was removed under reduced pressure. The crude product was purified by column chromatography (SiO_2, DCM + 5% MeOH, *v* / *v*) to yield **2** as a white solid (133 mg, 88%). Elemental analysis: Found: C, 72.59; H, 11.01; N, 4.90. Calc. for $C_{67}H_{121}BN_4O_7$: C, 72.79; H, 11.03; N, 5.07%. ^{1}H NMR (401 MHz, $CDCl_3$, Me_4Si): δ = 0.88 (t, ^3J = 6.9 Hz, 9 H, H-16/16'), 1.03 (t, ^3J = 7.3 Hz, 12 H, H-27), 1.22–1.38 (m, 48 H, H-8–15/8'–15'), 1.43–1.50 (tq, ^3J = ^3J = 7.3 Hz, 8 H, H-26; m, 6 H, H-7/7'), 1.60–1.91 (m, 18 H, H-6/6', H-19, H-20, H-25), 3.17–3.21 (m, 8 H,), 4.00 (t, ^3J = 6.6 Hz, 2 H, H-7), 4.01 (t, ^3J = 6.6 Hz, 4 H, H-7'), 4.11 (t, ^3J = 6.3 Hz, 2 H, H-21), 4.31 (t, ^3J = 6.2 Hz, 2 H, H-18), 7.24 (s, 2 H, H-2/2') ppm. ^{13}C NMR (101 MHz, $CDCl_3$, Me_4Si): δ = 13.8 (C_p, C-27), 14.3 (C_p, C-16), 19.8 (C_s, C-26), 22.8 (C_s, C-8–15/8'–15'), 24.0 (C_s, C-25), 25.5(7), 25.6 (C_s, C-19, C-20), 26.2(0) (C_s, C-7), 26.2(6) (C_s, C-7'), 29.4(7) (C_s, C-6'), 29.5(1), 29.5(4), 29.5(8), 29.7(3), 29.7(9), 29.8(1), 29.8(4), 29.8(5), 29.8(7), 29.8(9), 29.9 (C_s, C-8–15/8'–15'), 30.5 (C_s, C-6), 32.0(7), 32.0(8) (C_s, C-8–15/8'–15'), 59.1 (t, ^3J(^{15}N, ^{13}C) = 2.6 Hz, C-24), 62.3 (C_s, C-21), 64.8 (C_s, C-18), 69.3 (C_s, C-5'), 73.6 (C_s, C-5), 108.0 (C_t, C-2/2'), 125.1 (C_q, C-1), 142.4 (C_q, C-4), 152.9 (C_q, C-3/3'), 166.7 (C_q, C-17) ppm.

^{11}B NMR (128 MHz, $CDCl_3$): δ = –32.6 (s, 1 B) ppm. HRMS (MALDI) *m/z*: $[C_{51}H_{85}BN_3O_7]^-$ Calcd for $C_{51}H_{85}BN_3O_7$ 862.64861 (Chemdraw), 862.6475 (MALDI); Found 862.65147.

Sodium 18-crown-6 tricyano({4-[3,4,5-tris(dodecyloxy)benzoyloxy]butoxy}carbonyl)borate (**1a**)

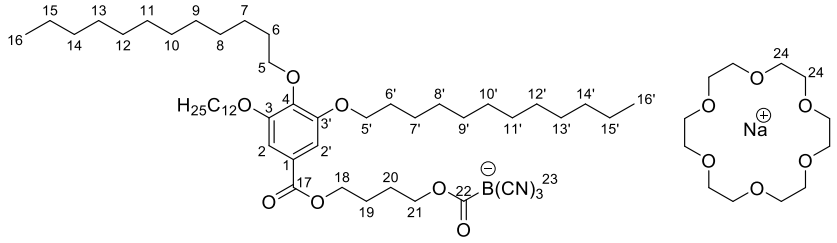

ILC **1a** was synthesized according to a modified literature procedure.[S4] Under nitrogen atmosphere, a solution of **6** (130.0 mg, 174 µmol, 1.1 eq.), $K[B(CN)_3CO_2H]$ (27.4 mg, 158 µmol, 1.0 eq.) and 18-crown-6 (83.6 mg, 316 µmol, 2.0 eq.) in dry DCM (1 mL) was slowly added to a solution of DPTS (82.7 mg, 281 µmol) and EDC (50 µL, 40 mg, 260 µmol) in dry DCM (1 mL). The solution was stirred at RT for 2 h. The solvent was removed under reduced pressure. The crude product was purified by column chromatography (SiO_2, DCM + 3% MeOH, *v* / *v*). Afterwards the product was dissolved in 2 mL DCM, Na_2SO_4 was added, and the solution was stirred for 12 h. This step was repeated two times by exchanging Na_2SO_4 to yield **1a** as a white solid (136.1 mg, 75%). ^{1}H NMR (401 MHz, $CDCl_3$) δ = 0.88 (t, ^3J = 6.9 Hz, 9 H, H-16/16'), 1.22–1.38 (m, 48 H, H-8–15/8'–15'), 1.43–1.50 (m, 6 H, H-7/7'), 1.60–1.91 (m, 10 H, H-6/6', H-19, H-20), 3.66 (s, 24 H,), 4.00 (t, ^3J = 6.6 Hz, 2 H, H-7), 4.01 (t, ^3J = 6.6 Hz, 4 H, H-7'), 4.12 (t, ^3J = 6.3 Hz, 2 H, H-21), 4.32 (t, ^3J = 6.2 Hz, 2 H, H-18), 7.24 (s, 2 H, H-2/2') ppm. ^{13}C NMR (101 MHz, $CDCl_3$) δ = 14.3 (C_p, C-16), 22.9 (C_s, C-8–15/8'–15'), 25.6(0), 25.6(4) (C_s, C-19, C-20), 26.2(2) (C_s, C-7), 26.2(7) (C_s, C-7'), 29.4(8) (C_s, C-6'), 29.5(3), 29.5(5), 29.5(9), 29.7(4), 29.8(0), 29.8(2), 29.8(4), 29.8(5), 29.8(7), 29.8(9), 29.9 (C_s, C-8–15/8'–15'), 30.5 (C_s, C-6), 32.0(8), 32.0(9) (C_s, C-8–15/8'–15'), 62.5 (C_s, C-21), 64.8 (C_s, C-18), 69.3 (C_s, C-5'), 69.4 (C_s, C-24), 73.6 (C_s, C-5), 108.0 (C_t, C-2/2'), 125.0 (C_q,

C-1), 142.4 (C_q, C-4), 153.0 (C_q, C-3/3'), 166.7 (C_q, C-17) ppm. ^{11}B NMR (128 MHz, $CDCl_3$): δ = –32.6 (s, 1 B) ppm. ^{23}Na NMR (106 MHz, $CDCl_3$) δ = –13.9 (s) ppm. (MHz, $CDCl_3$) HRMS (MALDI) *m/z*: $[C_{51}H_{85}BN_3O_7]^-$ Calcd for $C_{51}H_{85}BN_3O_7$ 862.64861 (Chemdraw), 862.6475 (MALDI); Found 862.64537. FT-IR: 2914 (s, -C-H stretch), 2849 (s, -C-H stretch), 1704 (s, -C=O stretch), 1686 (s, -C=O stretch), 1586 (m, -C=C- bending), 1333 (s, -C-O stretch), 1108 (s, -C-O stretch), 962 (s, -C=C-H deformation) cm^{-1}.

Potassium 18-crown-6 tricyano({4-[3,4,5-tris(dodecyloxy)benzoyloxy]butoxy}carbonyl)-borate (**1b**)

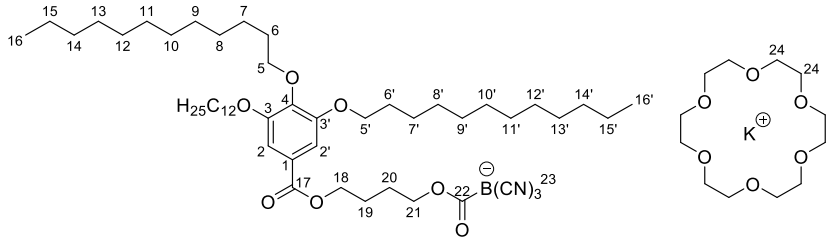

ILC **1b** was synthesized according to a modified literature procedure.[S4] Under nitrogen atmosphere a solution of **6** (70.0 mg, 93.7 µmol), $K[B(CN)_3CO_2H]$ (21.1 mg, 122 µmol) and 18-crown-6 (74.3 mg, 281 µmol) in dry DCM (1 mL) was slowly added to a solution of DPTS (82.7 mg, 281 µmol) and EDC (50 µL, 40 mg, 260 µmol) in dry DCM (1 mL). The solution was stirred at RT for 2 h. The solvent was removed under reduced pressure and the crude product was purified by column chromatography (SiO_2, DCM + 3% MeOH, *v* / *v*). Afterwards the product was dissolved in 2 mL DCM, K_2SO_4 was added, and the solution was stirred for 12 h. This step was repeated two times by exchanging K_2SO_4 to yield **1b** as a white solid (98.4 mg, 88%). ^{1}H NMR (401 MHz, $CDCl_3$) δ = 0.88 (t, ^3J = 6.9 Hz, 9 H, H-16/16'), 1.22–1.38 (m, 48 H, H-8–15/8'–15'), 1.43–1.50 (m, 6 H, H-7/7'), 1.60–1.91 (m, 10 H, H-6/6', H-19, H-20), 3.63 (s, 24 H,), 4.00 (t, ^3J = 6.6 Hz, 2 H, H-7), 4.01 (t, ^3J = 6.6 Hz, 4 H, H-7'), 4.12 (t, ^3J = 6.3 Hz, 2 H, H-21), 4.32 (t, ^3J = 6.2 Hz, 2 H, H-18), 7.24 (s, 2 H, H-2/2') ppm. ^{13}C NMR (101 MHz, $CDCl_3$) δ = 14.3 (C_p, C-16), 22.9 (C_s, C-8–15/8'–15'), 25.6(1), 25.6(3) (C_s, C-19, C-

20), 26.2(1) (C_s, C-7), 26.2(7) (C_s, C-7'), 29.4(7) (C_s, C-6'), 29.5(3), 29.5(5), 29.5(9), 29.7(4), 29.8(0), 29.8(2), 29.8(5), 29.8(6), 29.8(8), 29.9(0), 29.9(1) (C_s, C-8–15/8'–15'), 30.5 (C_s, C-6), 32.0(8), 32.0(9) (C_s, C-8–15/8'–15'), 62.4 (C_s, C-21), 64.8 (C_s, C-18), 69.3 (C_s, C-5'), 70.2 (C_s, C-24), 73.6 (C_s, C-5), 108.0 (C_t, C-2/2'), 125.0 (C_q, C-1), 142.4 (C_q, C-4), 152.9 (C_q, C-3/3'), 166.6 (C_q, C-17) ppm. ^{11}B NMR (128 MHz, $CDCl_3$): δ = –32.6 (s, 1 B) ppm. HRMS (MALDI) *m*/*z*: $[C_{51}H_{85}BN_3O_7]^-$ Calcd for $C_{51}H_{85}BN_3O_7$ 862.64861 (Chemdraw), 862.6475 (MALDI); Found 862.64531. FT-IR: 2913 (s, -C-H stretch), 2849 (s, -C-H stretch), 1706 (s, -C=O stretch), 1685 (s, -C=O stretch), 1587 (m, -C=C- bending), 1334 (s, -C-O stretch), 1105 (s, -C-O stretch), 961 (s, -C=C-H deformation) cm^{-1}.

3) NMR spectra of the target compounds 1a, 1b, 2 and intermediate 6

The assignment of the ^{1}H and ^{13}C signals was performed by 2D-NMR techniques (DEPT-135, COSY, HSQC, HMBC).

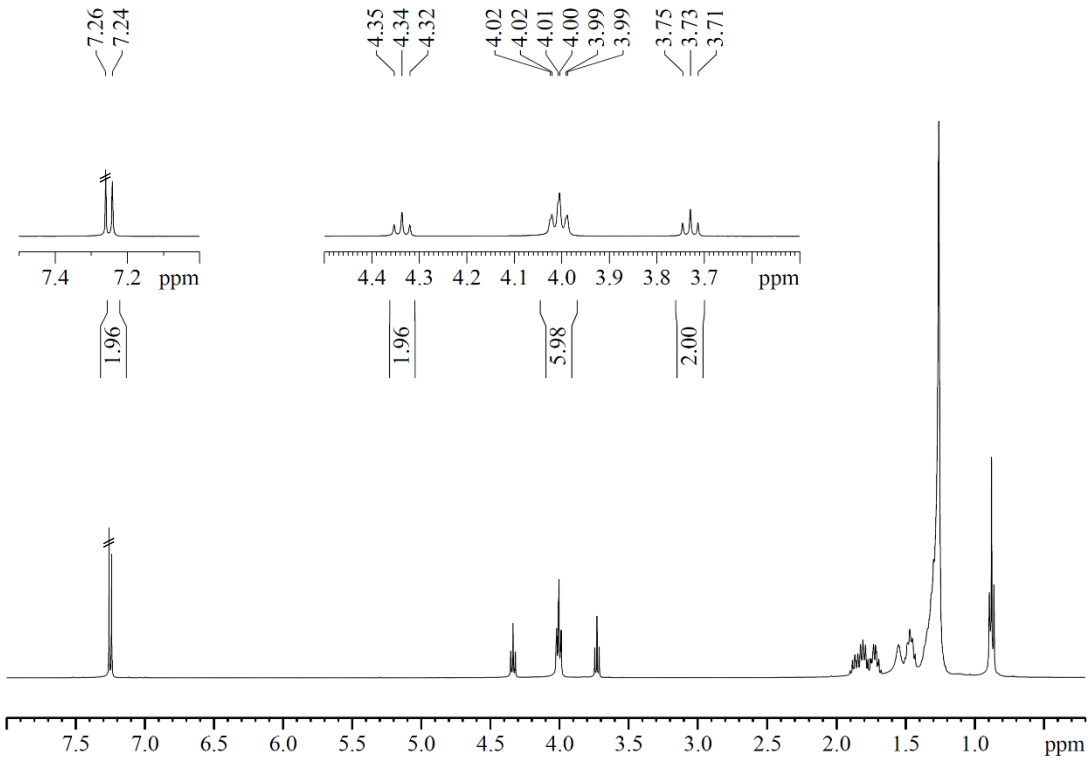

Figure S1. ^{1}H NMR spectrum ($CDCl_3$, 401 MHz) of compound **6**.

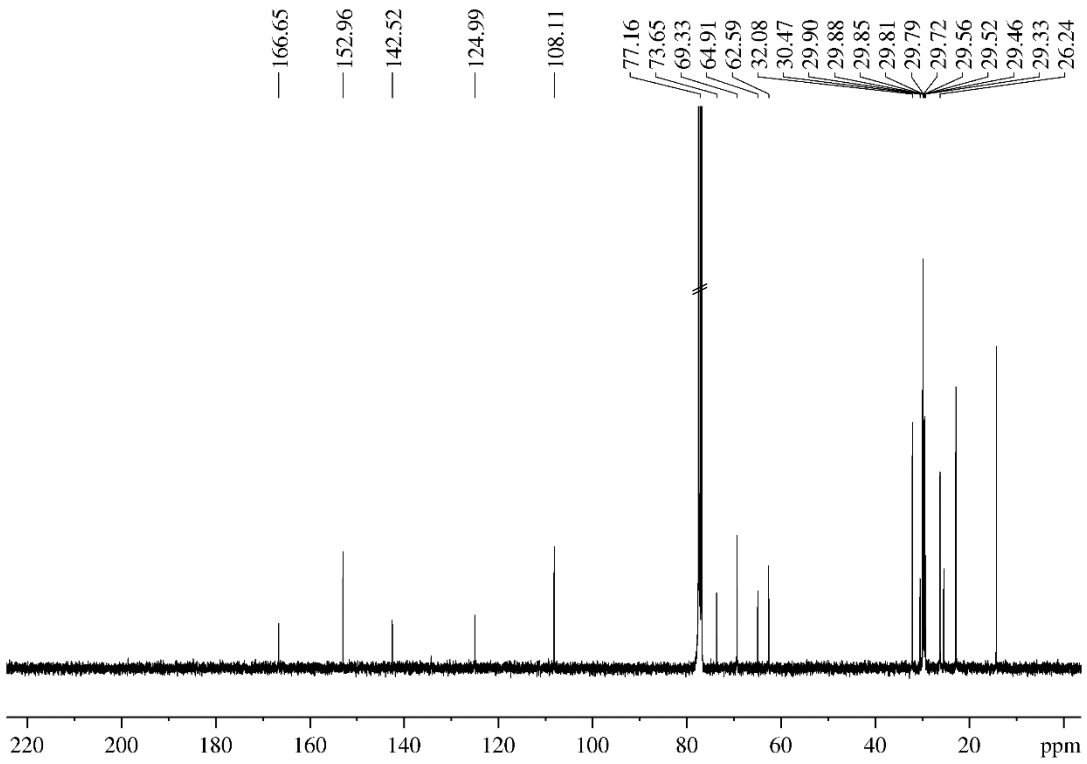

Figure S2. ^{13}C NMR spectrum ($CDCl_3$, 101 MHz) of compound **6**.

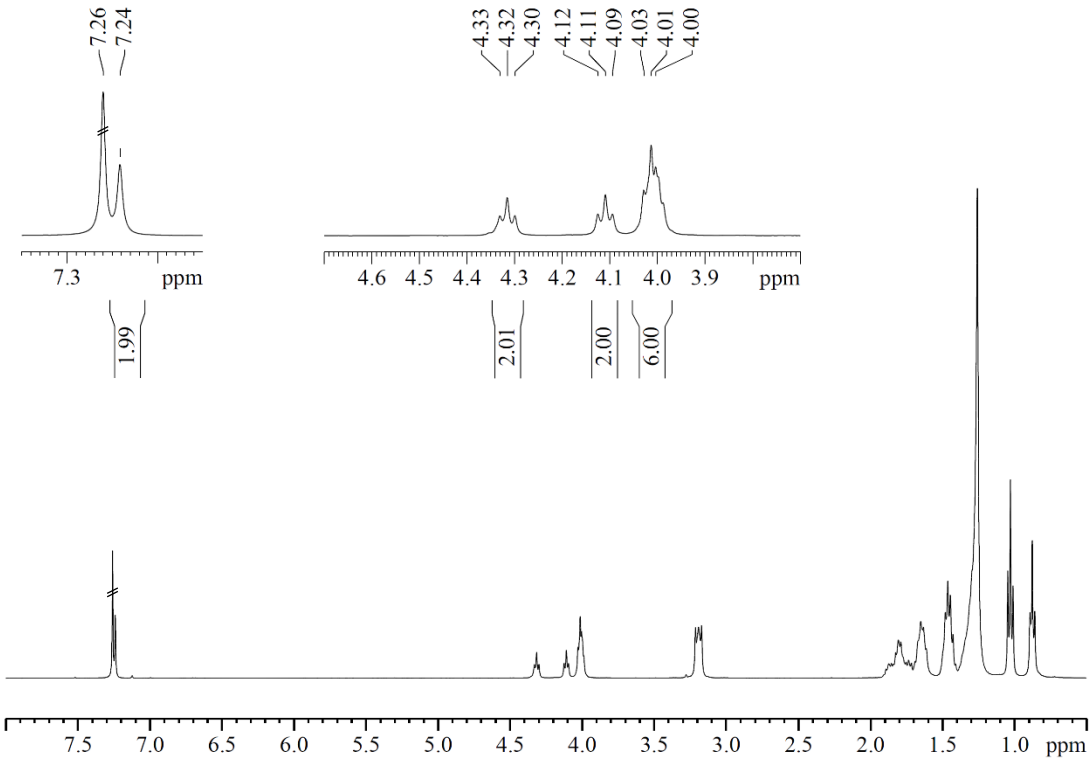

Figure S3. ^{1}H NMR spectrum ($CDCl_3$, 401 MHz) of **2**.

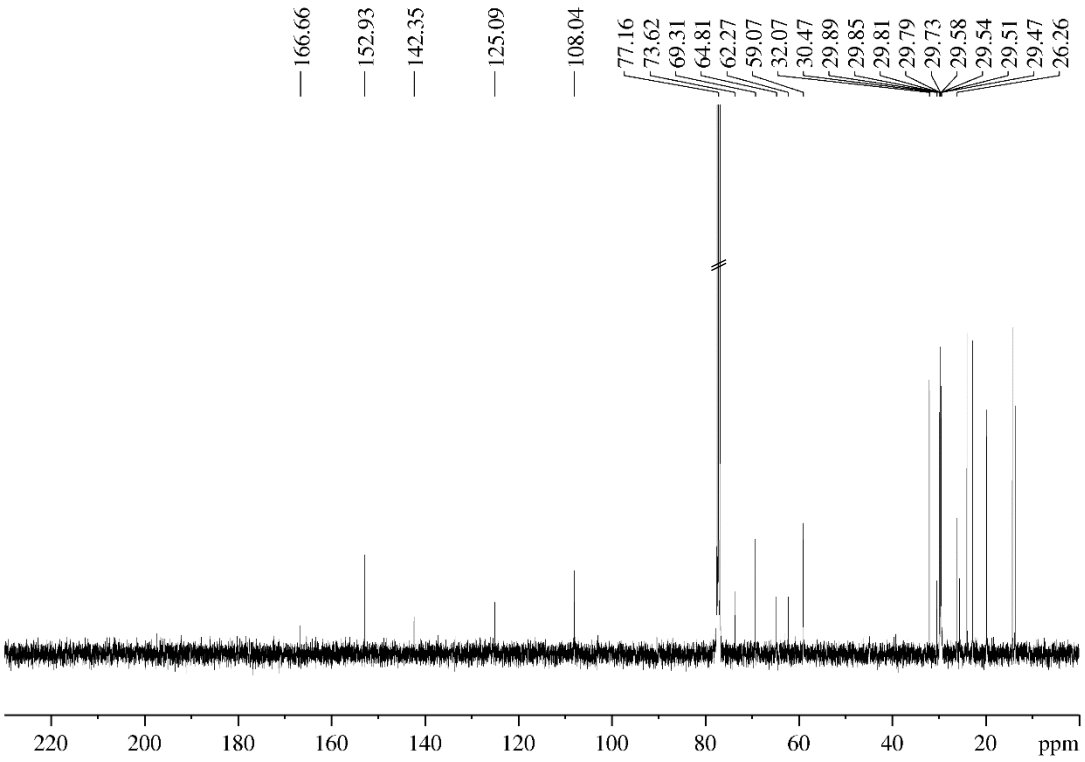

Figure S4. ^{13}C NMR spectrum ($CDCl_3$, 101 MHz) of compound **2**.

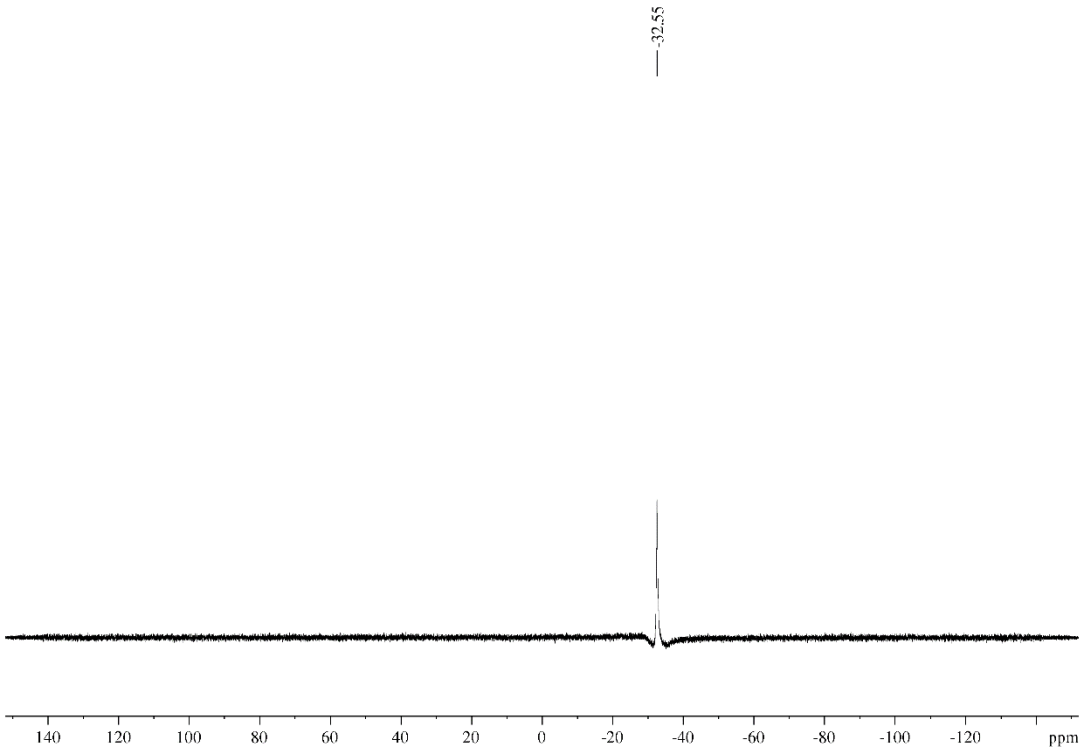

Figure S5. ^{11}B NMR spectrum ($CDCl_3$, 128 MHz) of compound **2**.

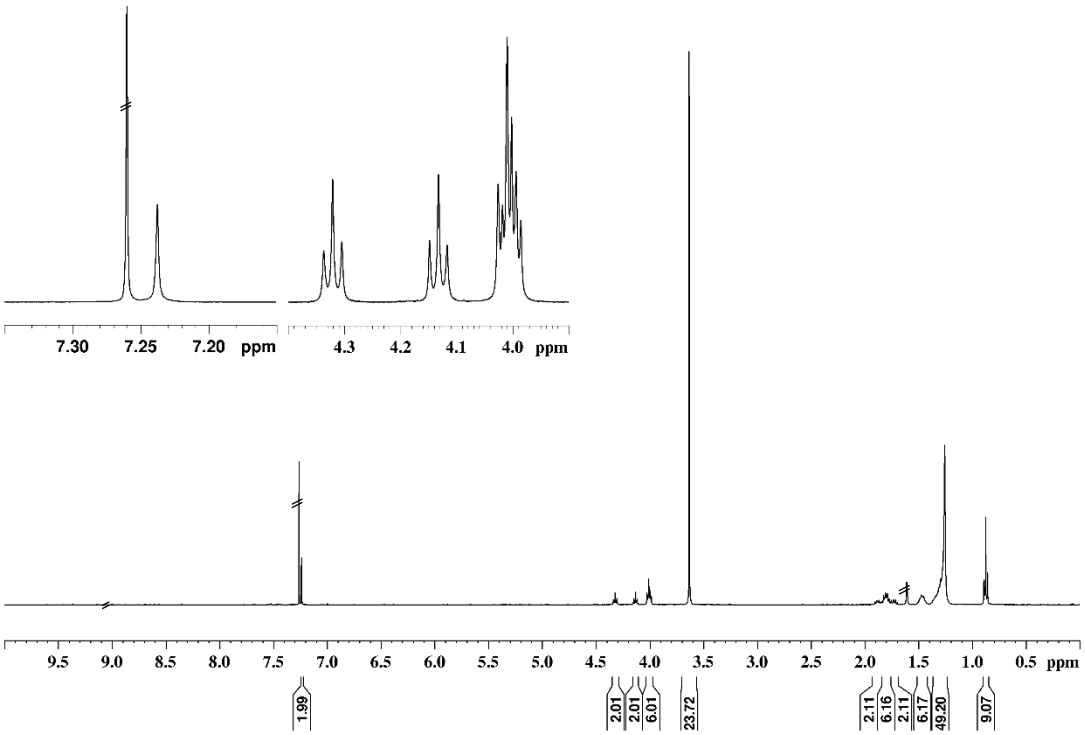

Figure S6. ^{1}H NMR spectrum ($CDCl_3$, 401 MHz) of **1b**.

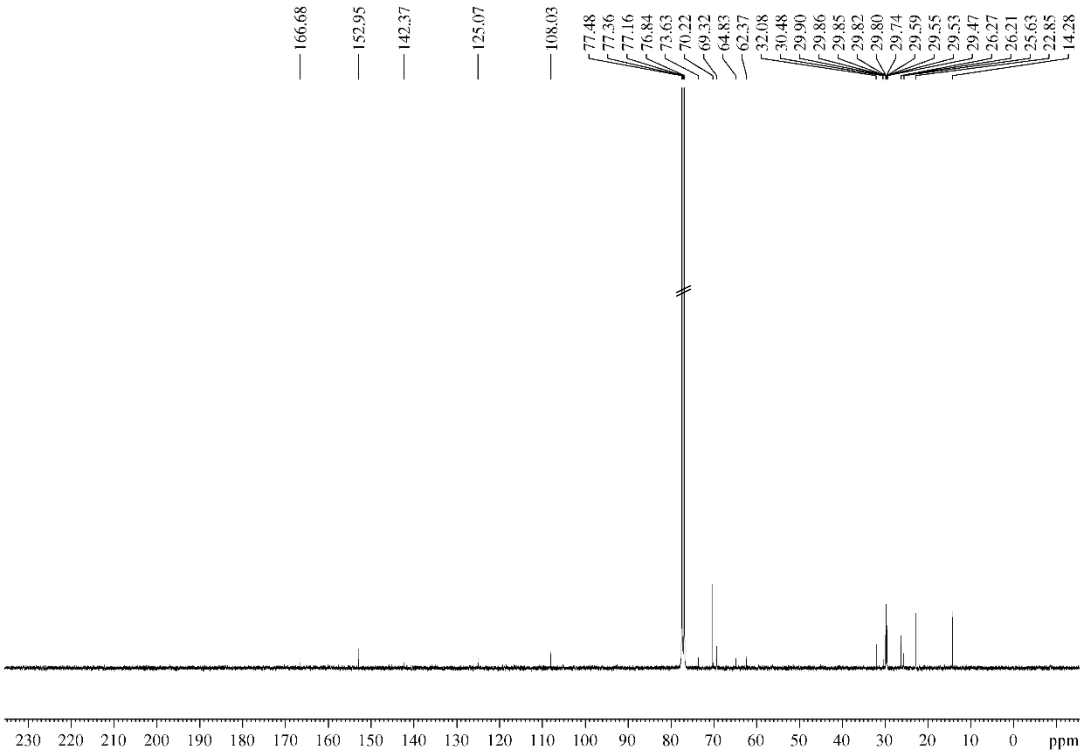

Figure S7. ^{13}C NMR spectrum ($CDCl_3$, 101 MHz) of compound **1b**.

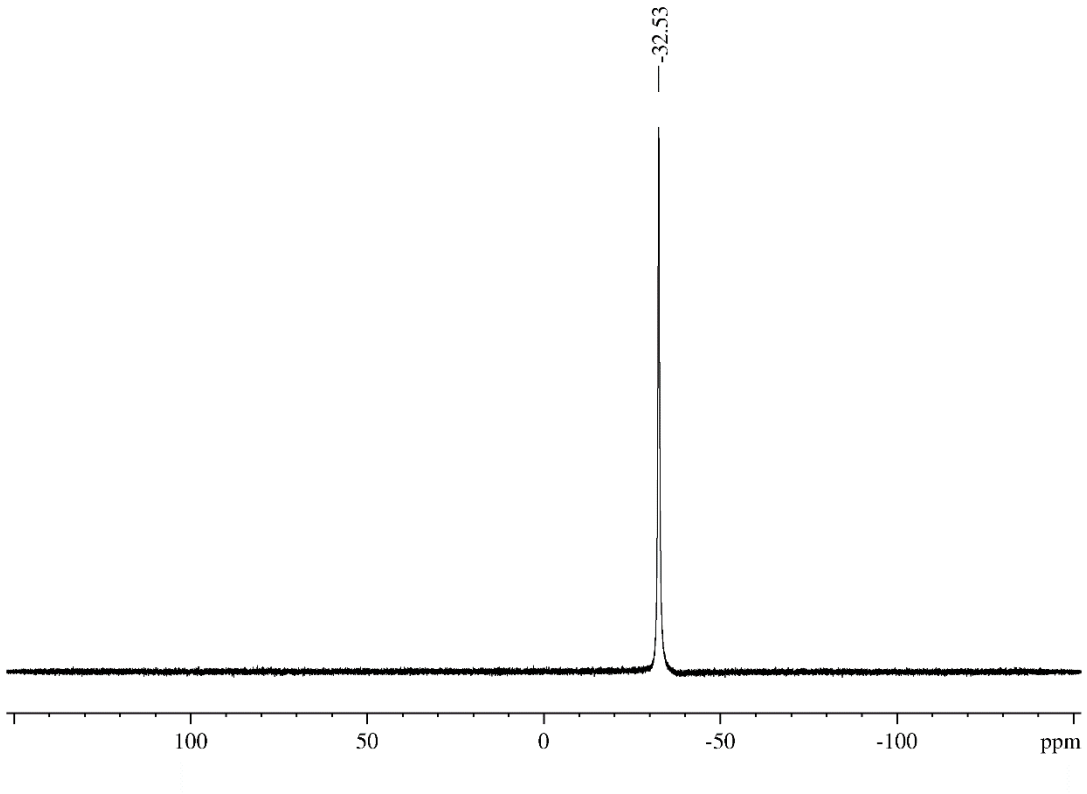

Figure S 8. ^{11}B NMR spectrum ($CDCl_3$, 128 MHz) of compound **1b**.

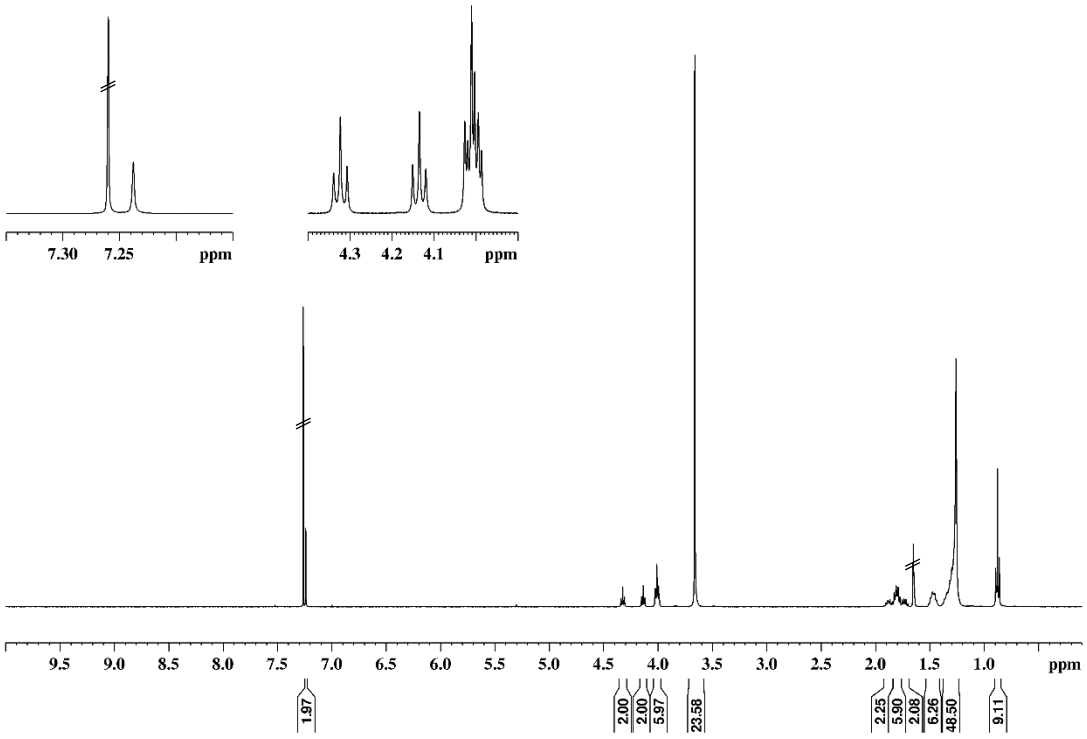

Figure S9. ^{1}H NMR spectrum ($CDCl_3$, 401 MHz) of **1a.**

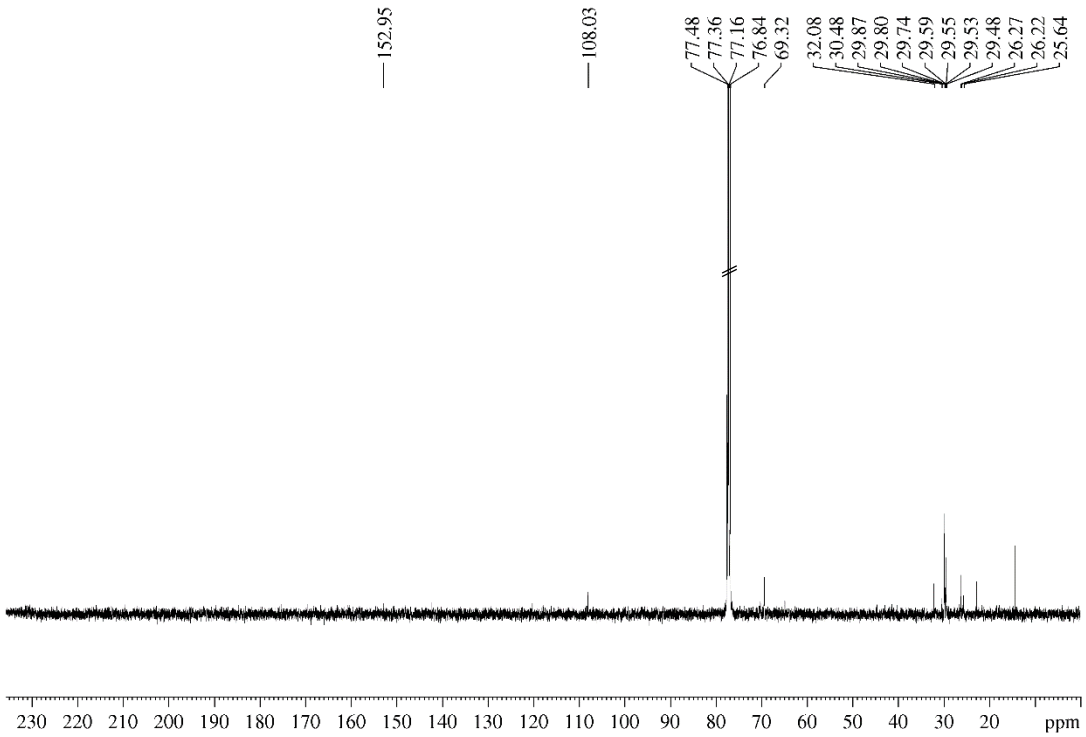

Figure S 10. ^{13}C NMR spectrum ($CDCl_3$, 101 MHz) of compound **1a**.

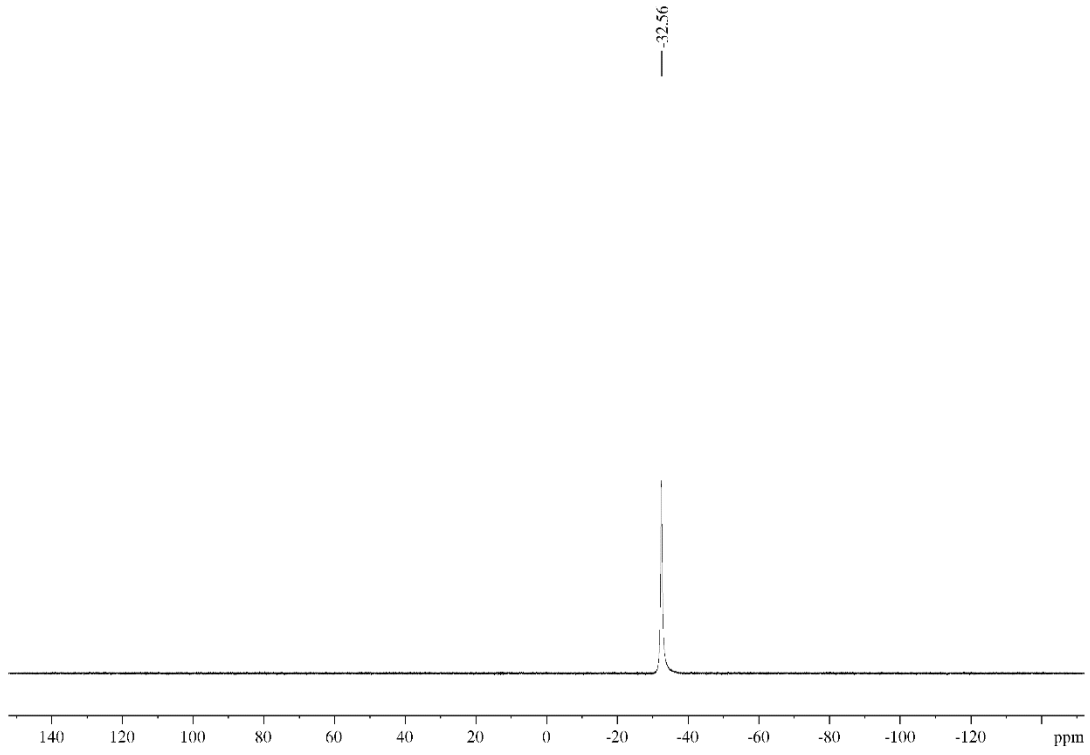

Figure S 11. ^{11}B NMR spectrum ($CDCl_3$, 128 MHz) of compound **1a**.

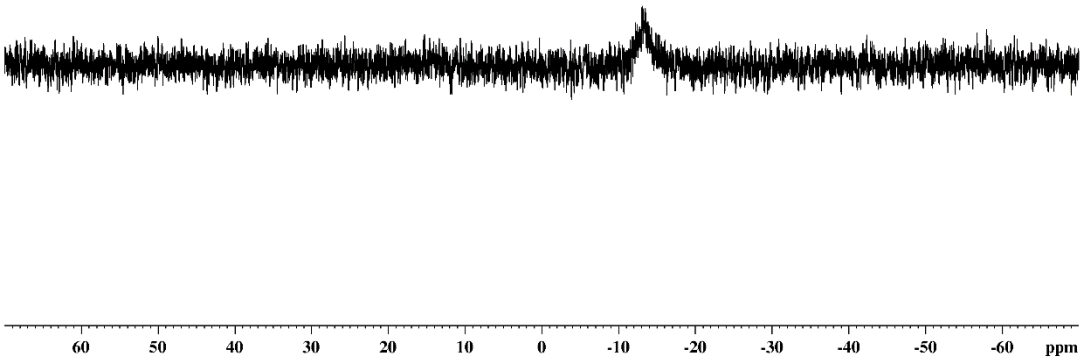

Figure S12. ^{23}Na NMR spectrum ($CDCl_3$, 106 MHz) of **1a.**

4) Polarised Optical Microscopy

a) Conoscopy images of ILC **2**

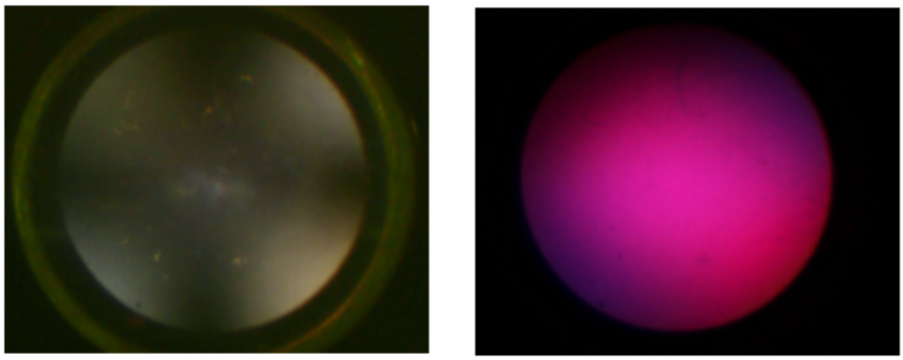

Figure S13. Conoscopy images of the homeotropically aligned phase of ILC **2** at 39.3 °C. Left: conoscopic cross. Right: Conoscopy with the compensation plate ($\lambda/2$). The colours in the quadrants confirm an optical positive mesophase.

b) POM observation of the SmA phase of ILC **1b**

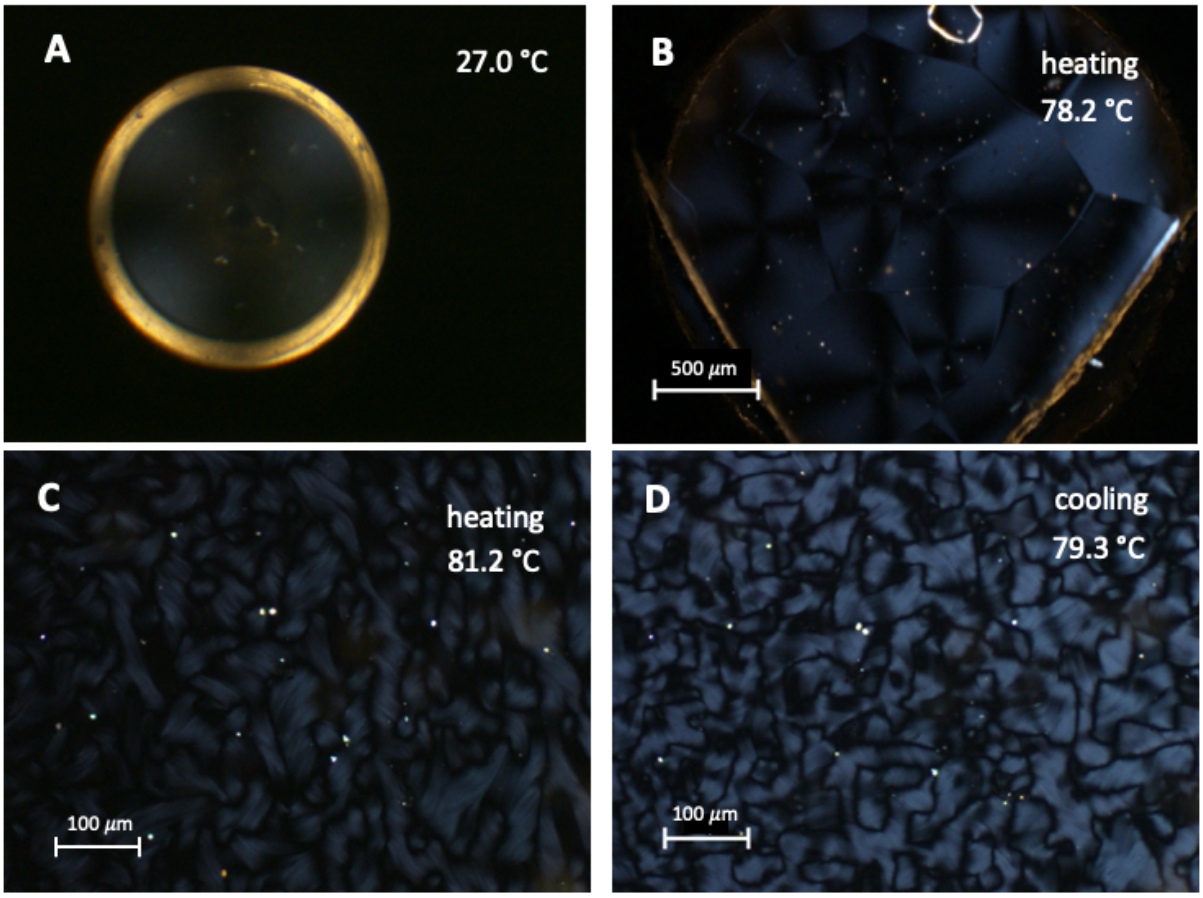

Figure S14. POM study of ILC **1b**. A Conoscopy of the homeotropically aligned SmA phase after cooling from 95 °C to 27 °C. B, C Textures after melting of the Cr_3 phase. D Texture at 79.3 °C after cooling the material from 85 °C.

The clearing transitions of ILC **1b** are invisible in DSC. However, POM studies exhibit the clearing transitions with characteristic textures above the melting temperature of the Cr_3 phase. If the material is cooled from 95 °C, which was frequently done to erase surface effects, the transition is visible as a transient bâtonnet texture which transforms quickly to a homeotropically aligned phase. This result makes it extremely difficult to observe the transition. However, the homeotropically-aligned SmA phase should show a conoscopic cross. In the thin film, the conoscopic image is weak and a conoscopic cross indicative for a uniaxial phase only becomes visible at low temperature (Figure 14 A). Upon heating the Cr_3 phase above 72 °C, a characteristic texture develops (Figure 14 B, C). If the temperature is not increased above 85 °C after clearing, a texture for the SmA phase is observed without the transition to a homeotropical-aligned material (Figure 14 D).

5) X-ray

a) *Crystalline Phases Cr_1 and Cr_2 and the SmA of compound **1a***

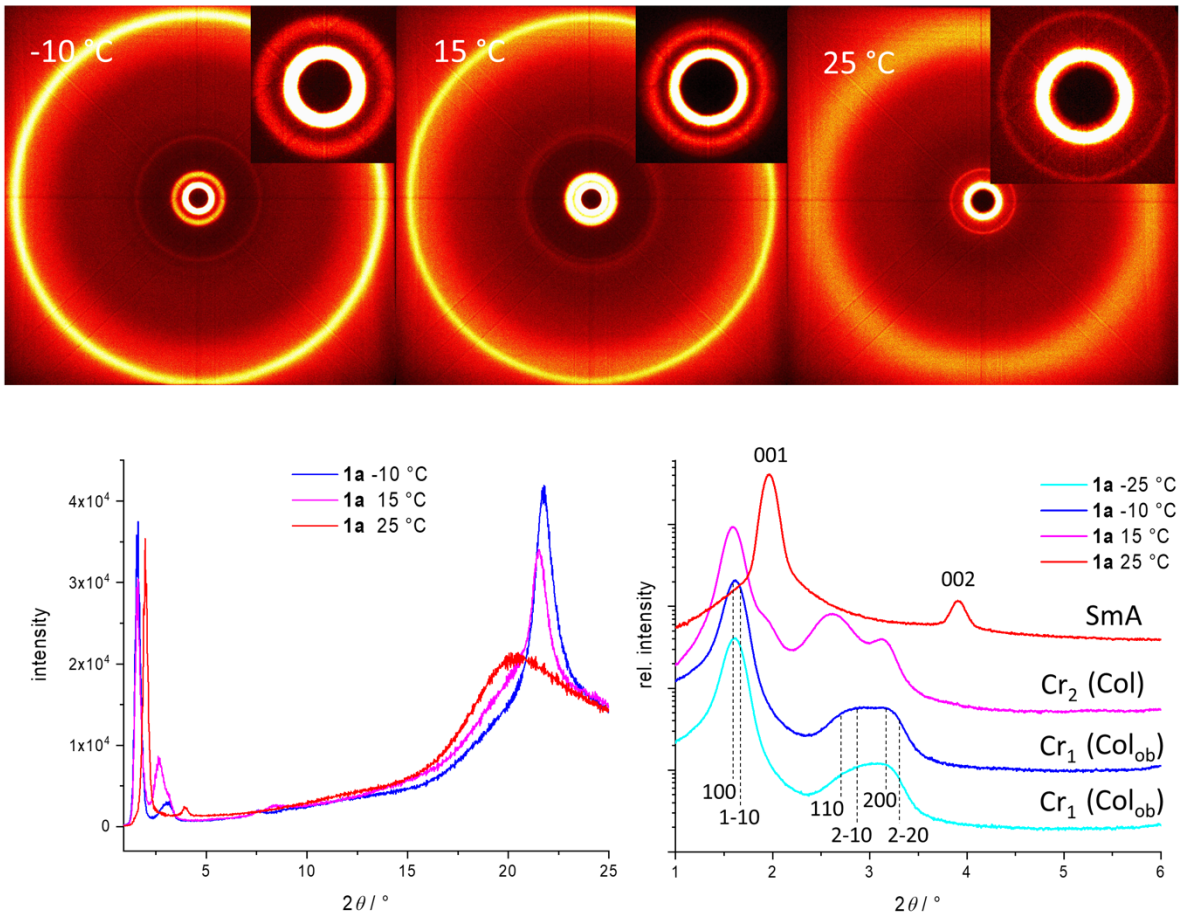

Figure S 15. WAXS diffraction pattern of ILC **1a** in the SmA phase (25 °C), the Cr_2 phase (15 °C) and the Cr_1 phase (−10 °C) and integration of MAXS pattern at −25 °C, −10 °C, 15 °C and 25 °C. Top: Powder pattern. Inset: Magnification of the small angle signals. Bottom left. Integration (2θ scan) of the patterns as the sum over the pixel intensities. Bottom right: Integration of the MAXS pattern with the reflection positions attributed to a distorted hexagonal columnar (Col_{ob}; ob = oblique) phase.

Table S1. WAXS data of **1a**.

T / °C	25	15	–10
d_{peak} / Å	-	4.13	4.13
ξ_{peak} / Å	-	19.9	18.5
I_{peak}	0	30046	43404
d_{halo} / Å	4.42	4.49	4.49
ξ_{halo}	3.2	5.9	4.6
I_{halo}	118317	26288	6684
$\%I_{halo}$	100	47	13

ξ_{peak} correlation length in units of d_{peak}; ξ_{halo} correlation length in units of d_{halo}; I_{peak}, I_{halo} intensities obtained by a fit of the area of the wide angle signals. $\%I_{halo} = I_{halo}/(I_{peak}+I_{halo})*100\%$.

Figure S15 show the transition from the SmA phase to the Cr_1 phase. The small angle signals become broader and are not equidistant anymore. Fibres of the material (Figure 3F) show the alignment of these signals on a single line indicating a two-dimensional columnar self-assembly. This are presumably hexagonal and distorted hexagonal (rhombohedral) phases, with a cell parameter of 63 Å. The breadth of the signals indicate a rather low correlation of the columns. The integration of the wide angle range highlights the driving force of the structure formation, which is the optimisation of the packing of the aliphatic chains (Table S1). The broad halo for the average distance of the fluid aliphatic chains at 4.4 Å in the SmA phase transforms stepwise to a pronounced signal assigned to a distance of 4.1 Å in the crystalline phases. At -10 °C, this signal dominates and the disordered portion (halo) attains only 13% of the total signal (Table S1). This demonstrates that upon cooling, the structure formation of the Cr_1 phase is mainly packing and rigidification of the liquid aliphatic chains and not the complete crystallisation of the structure. Therefore, the patterns do not show many reflections for Cr_1 or Cr_2 and are reminiscent of a soft disordered materials instead that of a highly-ordered crystal. Furthermore, it is assumed that the overall structure, i.e. the nanosegregation of the aliphatic and ionic parts, are similar in these phases.

b) *Crystalline Phases Cr_1 and Cr_3 and the SmA phase of compound* ***1b***

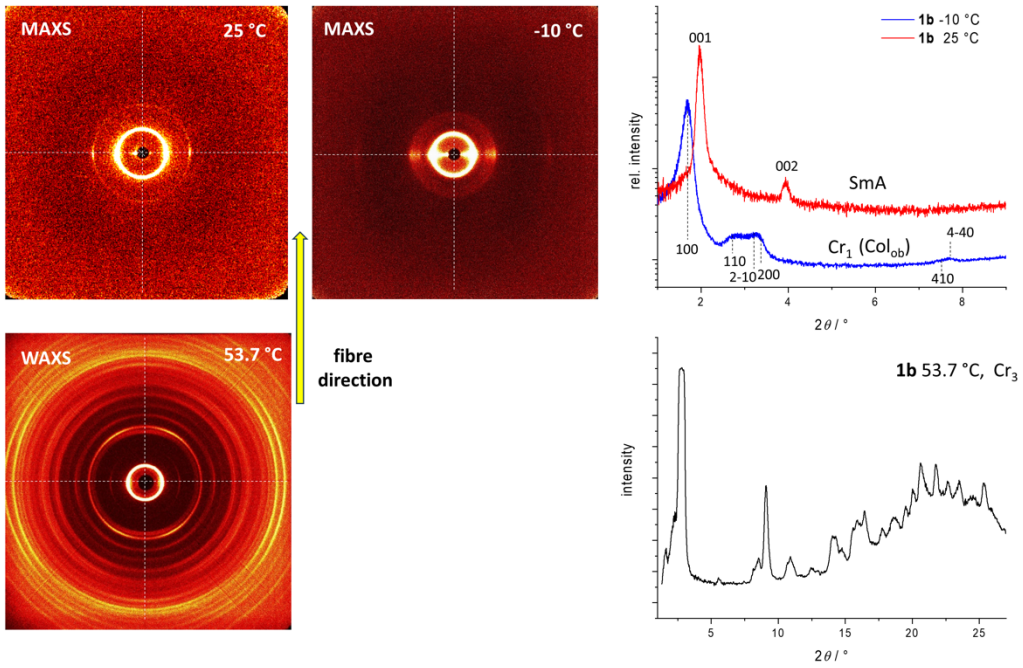

Figure S16. Top Left: MAXS diffraction pattern of a fibres of ILC **1b**, which is partially aligned along the fibre axis. Top Right: Integration of the pattern and indexation of the small angle reflections according to a SmA and a distorted hexagonal columnar (oblique) structure of the Cr1 phase. Bottom: WAXS diffraction pattern (left) and its integrated intensity (right) of the Cr_3 phase of ILC **1b**.

Figure S16 shows the middle angle diffraction pattern (MAXS), which could be partially aligned for ILC **1b**. The transformation from the SmA to the columnar Cr_1 phase does not change the alignment. This transition is reversible. There are no other strong reflections in the pattern of Cr_1 implicating that the molecules are not positional well ordered. This is in contrast to the highly-ordered crystal phase Cr_3 obtained when heating the material to 53.7 °C. The defined reflections over the entire angular range indicate a well-defined positional order of the molecules.

c) *Lamellar Crystalline Phase Cr_1 of ILC **2***

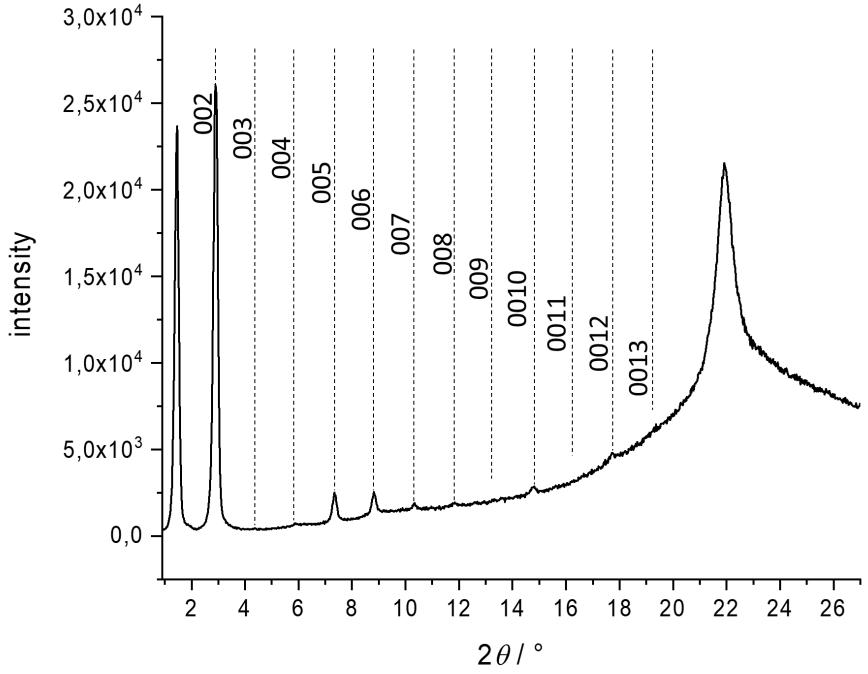

Figure S17. WAXS diffraction pattern of the lamellar crystal phase Cr_1 of ILC **2**.

Figure S17 shows the integrated intensity of the Cr_1 phase of ILC **2**. Here the lamellar structure of the SmA phase is maintained but the layer spacing is tremendously increased to 60.3 Å. Again, the packing of the aliphatic chains is the dominant factor by the structure formation, which is evident by the strong wide angle signal at 4.05 Å.

d) *X-ray tables*

Table S2. XRS results of ILC 2 (WAXS).

XRS results of ILC 2 (WAXS)						
Cr_1			c = 60.3 Å			
-10 °C	**h**	**k**	**l**	**d_{exp}** / Å	**d_{calc}** / Å	**Δ** / Å
	0	0	1	61.0	60.3	0.73*
	0	0	2	30.4	30.1	0.31*
	0	0	3	-	-	-
	0	0	4	15.0	15.1	0.08
	0	0	5	12.0	12.1	0.02
	0	0	6	10.0	10.0	0.02
	0	0	7	8.6	8.6	0.04
	0	0	8	7.5	7.5	0.06
	0	0	9	-	-	-
	0	0	10	6.0	6.0	0.03
	0	0	11	-	-	-
	0	0	12	5.0	5.0	0.01
meridian	halo			4.05	-	-
*WAXS diffraction superimposed with primary ray around beam stop, therefore the position deviates from the correct value. Correlation length according to Scherer: 52 nm i.e. 8-9 layers						
SmA			c = 43.9 Å			
25 °C	**h**	**k**	**l**	**d_{exp}** / Å	**d_{calc}** / Å	**Δ** / Å
equator	0	0	1	43.8	43.7	0.06
	0	0	2	21.7	21.9	0.12
meridian	halo			4.4	-	-
Correlation length according to Scherer: 42 nm i.e. 9–10 layers						
SmA			c = 43.4 Å			
35 °C	**h**	**k**	**l**	**d_{exp}** / Å	**d_{calc}** / Å	**Δ** / Å
equator	0	0	1	43.4	43.4	0.05
	0	0	2	21.5	21.7	0.15
meridian	halo			4.4		
Correlation length according to Scherer: 42 nm i.e. 9–10 layers						

Table S3. XRS results of ILC 1a (MAXS/WAXS).

XRS results of ILC 1a (MAXS/WAXS)						
Cr_1 (Col oblique)			a = b = 63.3 Å; γ = 117 °			
-10 °C	**h**	**k**	**l**	**d_{exp}** / Å	**d_{calc}** / Å	**Δ** / Å
MAXS	1	0	0	55.1	55.5	0.4
	1	-1	0	55.1	53.1	2.0*
	1	1	0	31.1	32.6	1.5*

	2	-1	0	31.1	31.1	0
	2	0	0	27.7	27.8	0.1
	2	-2	0	27.7	26.6	1.1*
	4	-3	0	14.7	14.8	0.1
	5	-4	0	11.7	11.6	0.1
	6	-1	0	9.8	9.9	0.1
WAXS	peak			4.1	-	
	halo			4.5	-	-
*reflections in principle allowed in the oblique unit cell. Owing to the very broad signals, no individual reflections are visible. They are either of low intensity or superimposed within the broad signal. Correlation length according to Scherer: 7 columns						
SmA			c = 45.0 Å			
25 °C	**h**	**k**	**l**	$\mathbf{d_{exp}}$ / Å	$\mathbf{d_{calc}}$ / Å	**Δ** / Å
MAXS	0	0	1	44.9	45.0	0.1
	0	0	2	22.6	22.5	0.1
WAXS	halo			4.4	-	-
Correlation length according to Scherer: 53 nm i.e. 11 layers						
SmA			c = 43.5 Å			
66.7 °C	**h**	**k**	**l**	$\mathbf{d_{exp}}$ / Å	$\mathbf{d_{calc}}$ / Å	**Δ** / Å
MAXS	0	0	1	43.1	43.1	0.0
	0	0	2	21.6	21.5	0.1
Correlation length according to Scherer: 51 nm i.e. 11 layers						

Table S4. XRS results of ILC 1b (MAXS/WAXS).

XRS results of ILC 1b (MAXS/WAXS)						
Cr_1 (Col_{ob} oblique)			a = b = 55.9 Å; γ = 110.4 °C			
-10 °C	**h**	**k**	**l**	$\mathbf{d_{exp}}$ / Å	$\mathbf{d_{calc}}$ / Å	**Δ** / Å
MAXS	1	0	0	52.7	52.4	0.3
	1	1	0	31.3	31.9	0.6
	2	-1	0	27.0	27.6	0.6
	2	0	0	27.0	26.2	0.8*
	4	1	0	11.6	11.8	0.2
	4	-4	0	11.6	11.5	0.1
WAXS	peak			4.1	-	
	halo			4.5	-	-
*reflections in principle allowed in the oblique unit cell. Owing to the very broad signals, no individual reflections are visible. They are either of low intensity or superimposed within the broad signal. Correlation length according to Scherer: 380 nm i.e. 7 columns						
SmA			c = 44.8 Å			
25 °C	**h**	**k**	**l**	$\mathbf{d_{exp}}$ / Å	$\mathbf{d_{calc}}$ / Å	**Δ** / Å

MAXS	0	0	1	44.8	44.8	0.1
	0	0	2	22.4	22.4	0.1
WAXS	halo			4.3	-	-
Correlation length according to Scherer: 65 nm i.e. 14.5 layers						
SmA			*c* = 43.3 Å			
53.6 °C	**h**	**k**	**l**	$\mathbf{d_{exp}}$ / Å	$\mathbf{d_{calc}}$ / Å	**Δ** / Å
MAXS	0	0	1	43.3	43.3	0.0
	0	0	2	21.7	21.7	0.0
WAXS	halo			4.4	-	-
Correlation length according to Scherer: 67 nm i.e. 15.6 layers						

d) Schematic model of the columnar phases

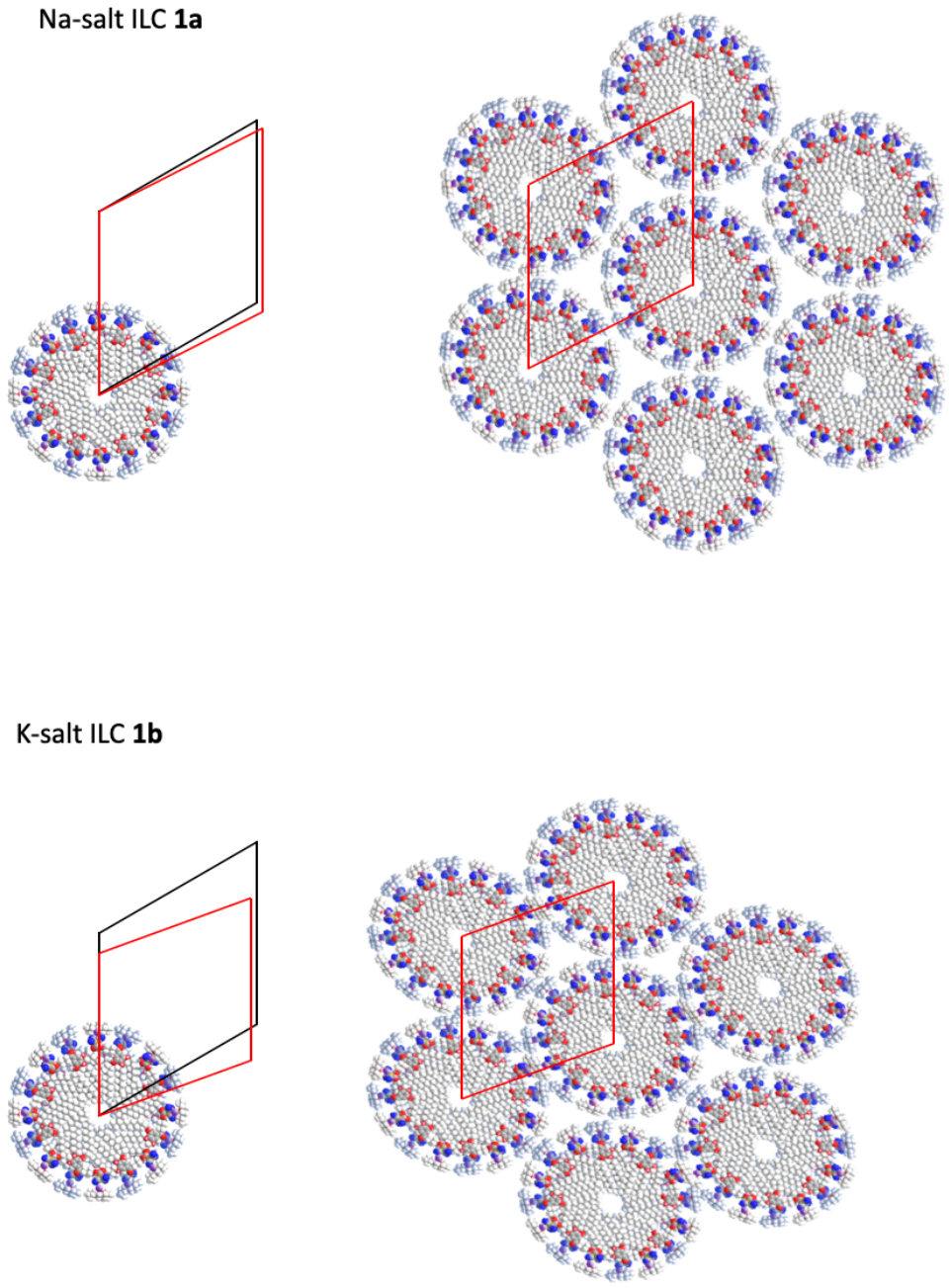

Figure S18. Schematic model of the columnar phases of ILCs **1**. Left. Columnar unit with a diameter of 63.3 Å and the oblique unit cell (red) is compared with the hexagonal unit cell (black). For the sodium derivative **1a** the cell is a slightly distorted hexagonal cell, while for ILC **1b** the distortion is larger. The deviation from the hexagonal symmetry can be rationalised with an elliptical cross section of the columns.

6) Electron density reconstruction

The electron density was reconstructed by a 2θ scan and the Sum integration with datasqueeze.[S1] The reflections were fitted with the same program to obtain the peak area as the total intensity. These intensity values were used with the program "electron_density-map.exe" provided by the courtesy of Prof. Carsten Tschierske (University of Halle, Germany).

For the reconstruction of the SmA phases only the intensities of the 001 and 002 reflections were available. For the reconstruction of the lamellar Cr_1 phase of ILC **2,** the four reflections of higher intensity (001, 002, 005, 006) have been considered. Additionally, the electron density and the density were calculated for the different sections in the electron density pattern. The number of molecules in the area of 31 Å * 31 Å in the layer have been restricted to 18 molecules in the SmA phase in order not to exceed the density of 1 gcm^{-3} of the aliphatic chains, which would be in the range of the density of crystalline polyethylene.[S5] The number of molecules in the Cr_1 have been chosen to attain a density close to 1 gcm^{-3}, which is typical for soft organic matter. An experimental density could not be measured by the buoyancy method owing to the amphiphilic nature of the ILCs, which either dissolve or swell in all solvents.

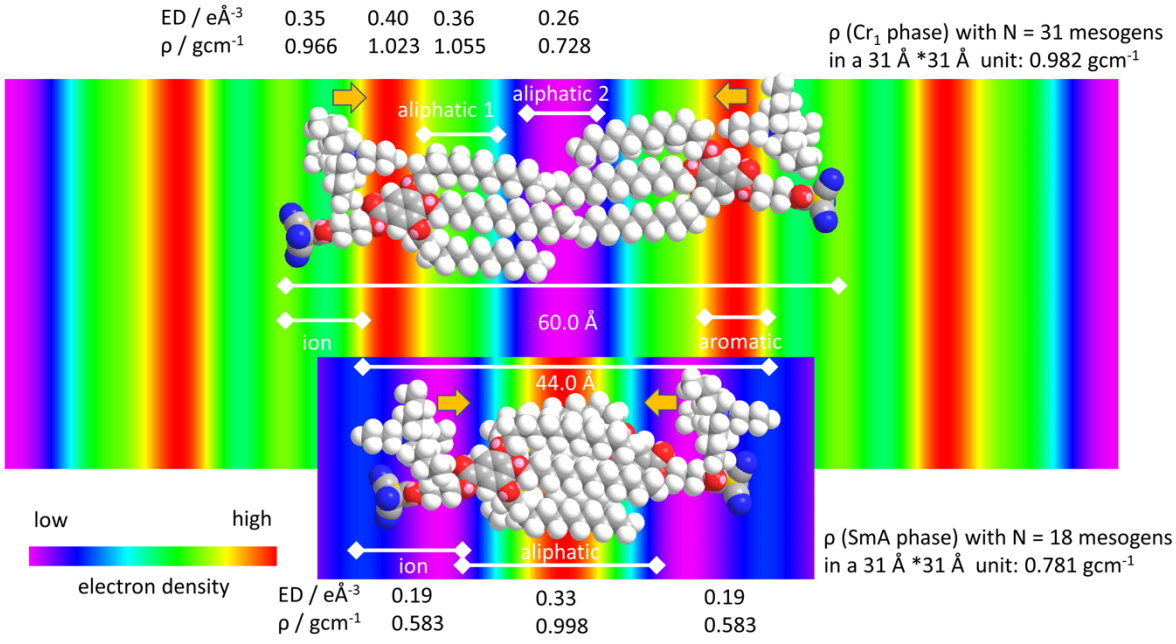

Figure S19. Electron density reconstruction of the Cr_1 phase of ILC **2** and comparison with the electron density in the SmA phase of ILC **2**.

Figure S19 highlights the comparison of the electron density in the SmA and the Cr_1 phase of ILC **2**. In the bilayer SmA (SmA_2) phase, the layer spacing can be only rationalised by the

interdigitation of all aliphatic chains. With this molecular model, the electron densities and the densities can be calculated for all the different sections. This results in the middle of the bilayer in the highest electron density and also in the highest density, while the lowest electron density and the lowest density can be calculated in the spacer section with the ammonium ions. This model is fully consistent with the electron density reconstruction from the XRS intensities. Upon formation of the crystal phase (Cr_1), the layer spacing increase by the length of a dodecyl chain, thus it is reasonably that the chains separate resulting in the absence of any interdigitation. The bilayer of molecules fit perfectly on top of the reconstructed electron density obtained from XRS. When subsequently calculating the electron densities and densities with the molecular model, the changes fit very well with the changes in the reconstructed electron density pattern, confirming the validity of the model. Note that the density of the ionic section in the SmA_2 phase is low, which explain the relatively high conductivity of the mobile charge carriers in this phase. For the Cr_1 phase, this density almost doubles and rationalise the complete absence of conductivity in the crystalline phase. It is important to mention that with NMR methods, the position of the ammonium ions within the spacer region has been confirmed for the Cr_1 phase (see next section). Generally, it is not immediately clear that this organization necessarily continues in the SmA_2 phase. However, the change of the layer spacing, the electron density, the reversible formation of the SmA phase from the Cr_1 / Cr_2 phase and the most prominent change of the WAXS signal at 4.1 Å all point to the prominent contribution of the packing of the aliphatic chains at this transition and indicate that the position of the ammonium cation continues into the liquid crystal phase, as shown in the model.

Electron density reconstruction was not possible for the columnar phases of compounds **1a** and **1b** owing to overlapping and broad reflections (see Figure S15 and S16). Therefore, only schematic models have been produced (Figure S18).

7) Solid State NMR

NMR measurements

^{1}H, ^{11}B and ^{13}C CP and DE solid-state NMR spectra of **1a** and **1b** were recorded on a Bruker Avance 600 MHz spectrometer (14.1 T) with a double channel 3.2 mm probe and a spinning speed of 10 kHz. The set temperature was 243.0 K to 250 K, although the temperature is increased +10 °C due to frictional heating during MAS. Solid-state NMR measurements of **2** were recorded on a Bruker Avance Neo Spectrometer (9.4 T) using a 4 mm double channel HX probe at 268 K and spinning speed of 8 kHz. The magic angle was calibrated with KBr and α-glycine was used to set the ^{1}H 90° pulse. For cross polarization (CP) experiments a 90 to 100 ramp and SPINAL-64 for heteronuclear decoupling was used. Adamantane was used to reference the chemical shift. Data evaluation was done with Bruker software TopSpin 4.3.0.

Specific Sample Preparation

The samples were packed in the rotor. The subsequent heating and cooling process imitated the temperature settings used to generate the sample for the X-ray measurements. First, the sample was heated to the isotropic phase. After several minutes the samples were cooled to room temperature and then stored in a box cooled with solid CO_2.

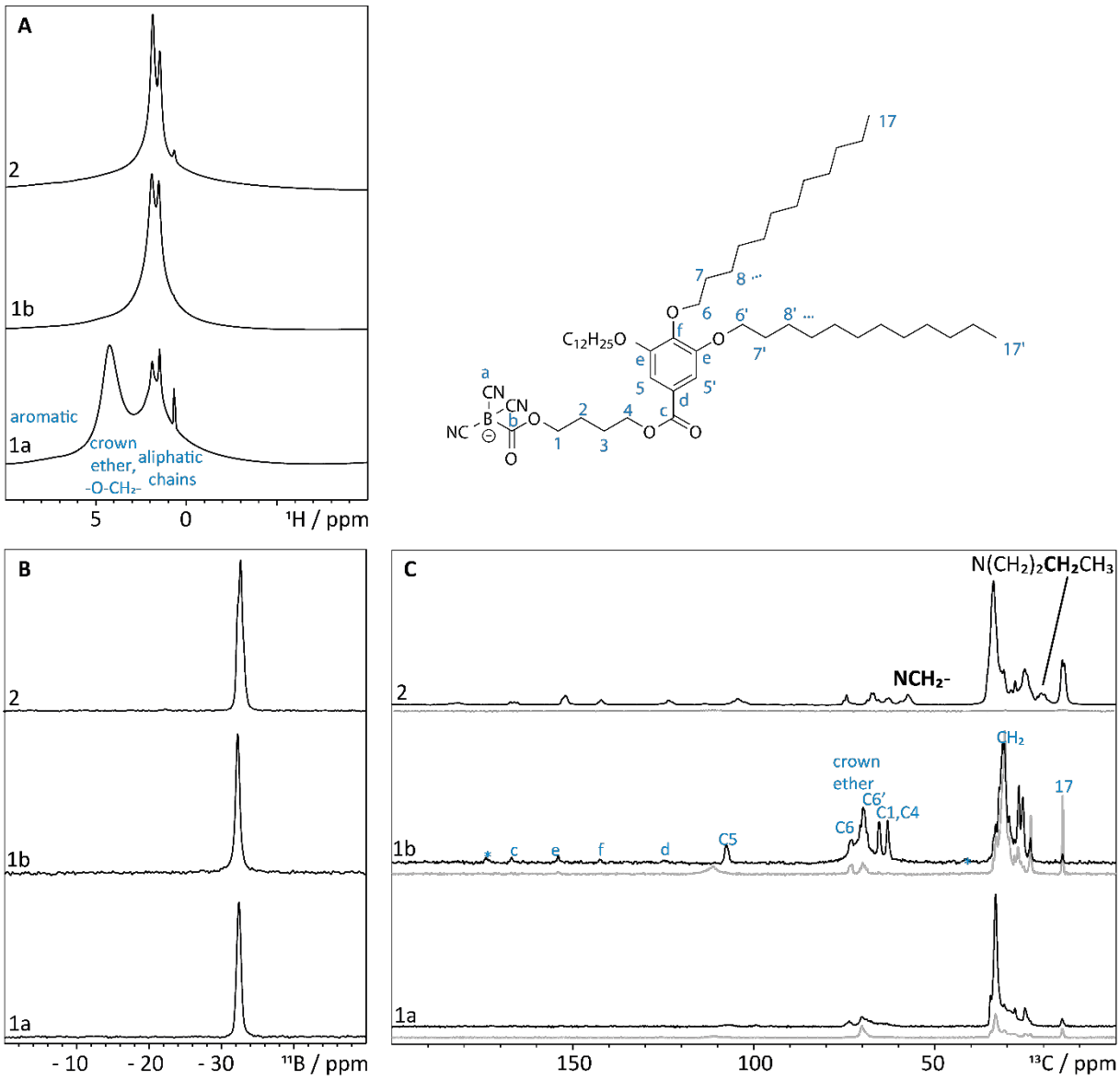

Figure S20. Samples **1a** and **1b** were measured at 250 K and 10 kHz, whereas **2** was measured at 268 K and 8 kHz. A) ^{1}H solid-state NMR spectra recorded with 16 scans and a recycle delay of 2 s. B) ^{11}B hahn-echo spectra of **1a** (–32.4 ppm) and **1b** (– 32.3 ppm) @ 253 K, 10 kHz MAS, 16 scans and a recycle delay of 20 s. The boron signal is narrow due to the tetrahedral coordination of the quadrupolar ^{11}B nucleus. C) ^{13}C CPMAS (black) spectra were recorded with 5120 scans (**1a** and **1b**) and 10240 scans (**2**), a recycle delay of 2 s and a contact time of 2 ms. The ^{13}C DEMAS (grey) spectra were recorded with 1024 scans (**1a** and **1b**) and 256 scans (**2**), and a short recycle delay of 1 s (**1a** and **1b**) and 2 s (**2**), to specifically probe signals with a higher mobility.

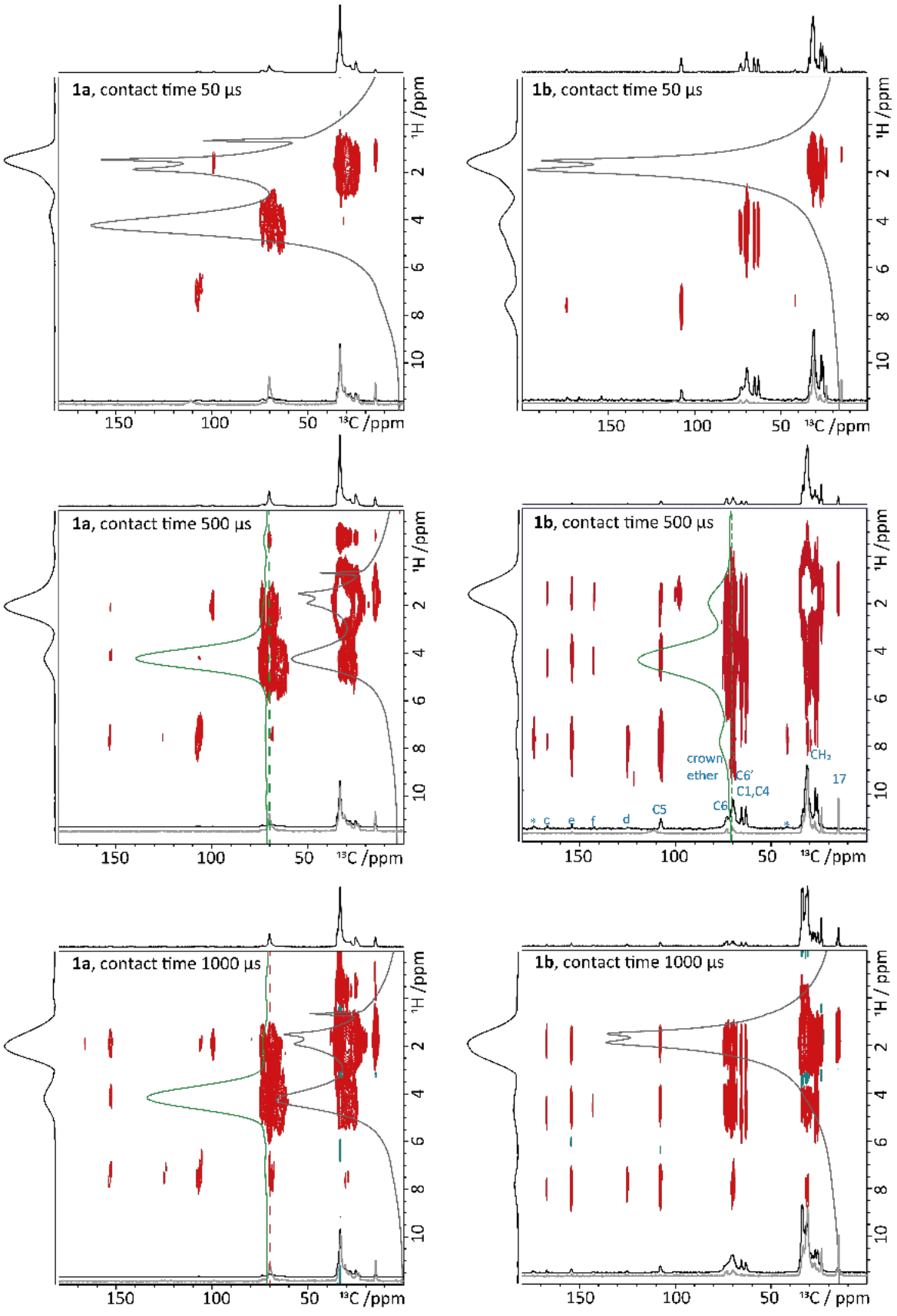
1a, contact time 50 µs
1b, contact time 50 µs
1a, contact time 500 µs
1b, contact time 500 µs
1a, contact time 1000 µs
1b, contact time 1000 µs
¹H /ppm
¹³C /ppm
crown ether
C6'
C1,C4
C6
C5
CH₂
17
c
e
f
d

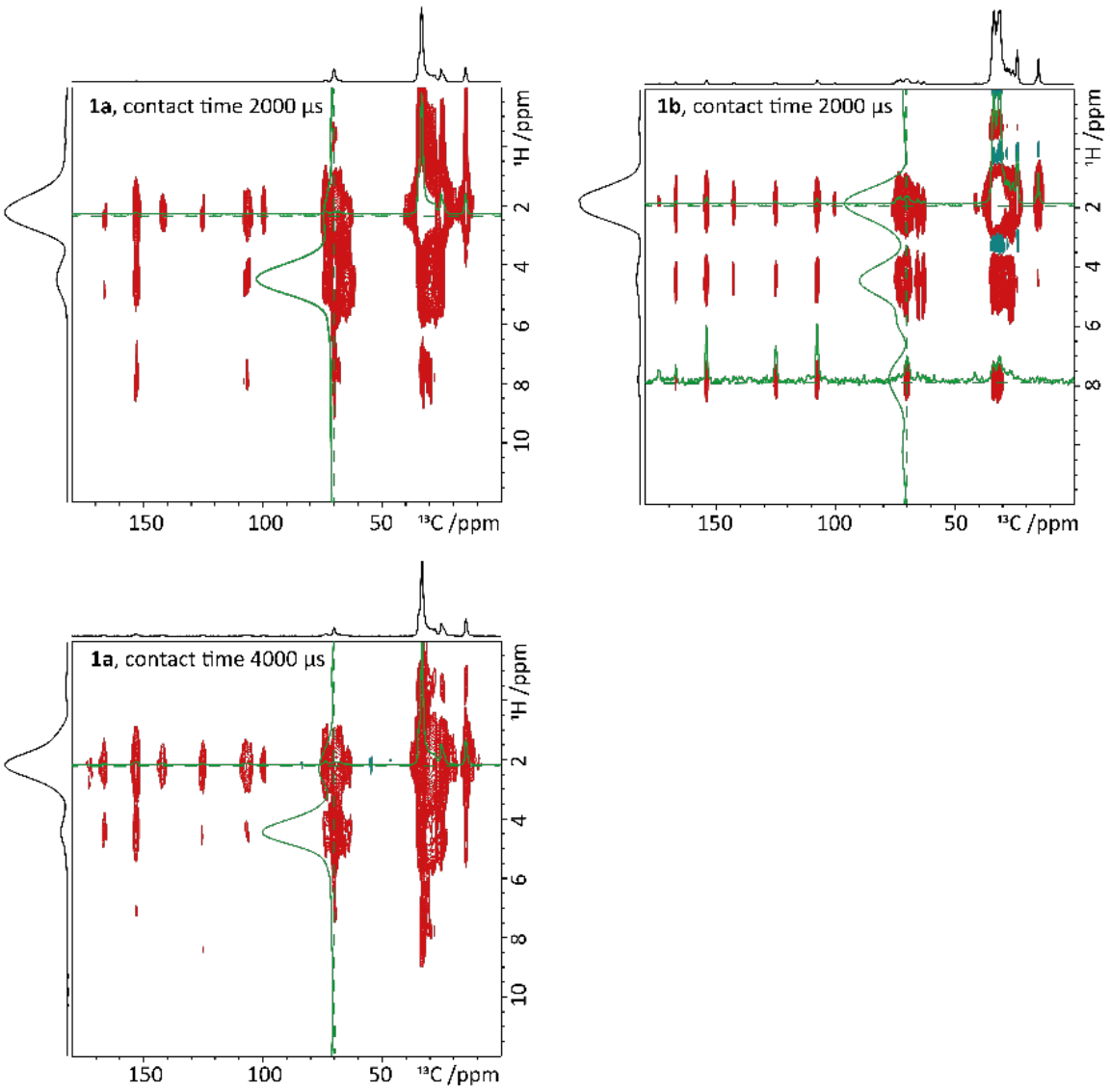

Figure S21 (previous page and here): ^{1}H-^{13}C FSLG HETCOR spectra of **1a** and **1b** measured at 245 and 250 K and 10 kHz MAS with different contact times. For compound **1a** spectra with a contact time of 1000 µs, 2000 µs and 4000 µs were processed using forward linear prediction of 100, 100 and 125 additional t_1 FIDs. For spectrum **1b** with a contact time of 50, 1000 µs, 2000 µs forward linear prediction of 140, 70 and 100 additional t_1 FIDs was used.

Crystalline phase Cr_3 of 1b

1a can exist in different crystalline forms, which was observed by DSC measurements. To be sure that the crystalline phase Cr_1 is analyzed by solid-state NMR, the crystalline phase Cr_3 was also prepared. To obtain the crystal form Cr_3 of **1b,** the sample was heated to 90 °C, cooled down to -30 °C and then heated again to 45°C. After several minutes, the sample was cooled down on solid CO_2 and stored under these conditions until the solid-state measurements were performed at 253 K.

Crystal structure Cr_3 of **1b** shows the signals of Cr_1 and additional signals in the signal area of the aliphatic chains and several chemical environments for the methyl group. The linker molecules remain immobile.

The signals lead to the conclusion that the phase Cr_3 is a mixture of the crystal phase Cr_1 and an additional phase with higher mobility, which could be in a similar arrangement to the crystal phase Cr_1 of **1a**.

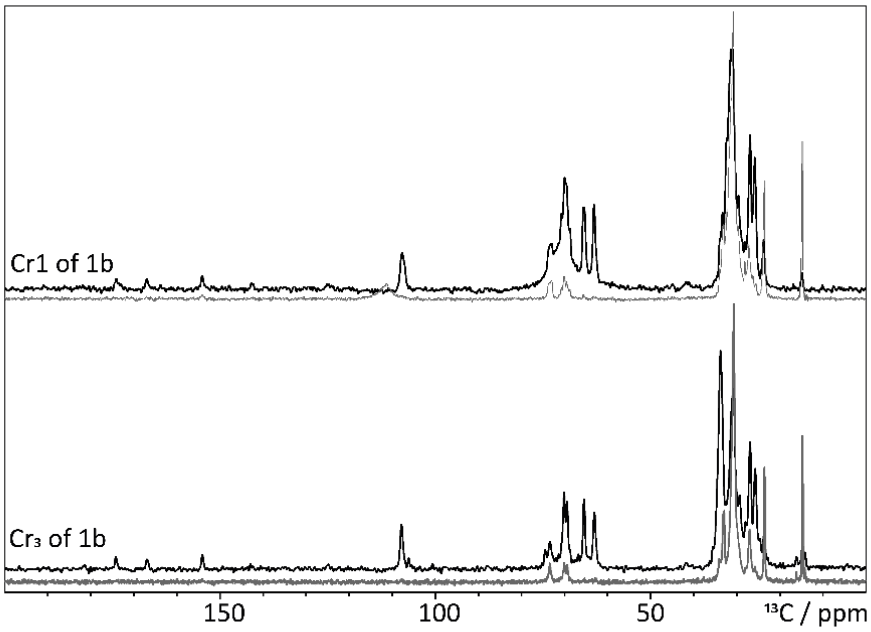

Figure S22. ^{13}C CPMAS (black) and DE (grey) spectra of **1b** in phase Cr_1 and Cr_3 recorded with 5120 scans, a recycle delay of 2 s and 1024 scans with a recycle delay of 1 s, respectively.

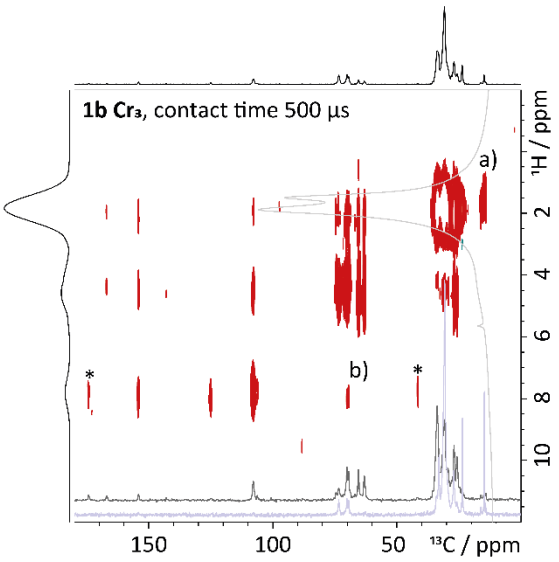

Figure S23. ^{1}H-^{13}C HETCOR spectrum of **1b** Cr3 with a contact time of 500 µs. For the overlapping signals at $\delta(^{13}C) = 70$ ppm it cannot be distinguished whether the spatial proximity to the aromatic as well as to the aliphatic structural components (denoted as (b)) results from C6/C6', the crown ether or both.

8) Modelling

General

Molecular models for the liquid crystalline phases were set up on the basis of the X-ray data of the SmA or Cr_{Lam}. The phases were modeled with the program *BIOVIA Materials Studio 2017 R2*. The modeling was performed in the P1 unit cell without symmetry restrictions. Since the experimental data only provides the *c* parameter, a section of the layer was assembled using a and b parameters resulting in a matrix containing 2 x 3 x 3 mesogens in a double layer with a density of 0.98 gcm^{-3}. After the set-up of the unit cells, the geometry optimization was performed using the module "Forcite Plus (2017R2)" with the force field "Universal" and the atom-based summation method until the non-covalent interactions (electrostatic and van der Waals interactions) were large and negative.

*a) Model of the LC phase of ILC **1a** at 25 °C*

Nine ILCs **1a** have been placed side by side in a P1 unit cell with rectangular symmetry (a = 31.00 Å, b = 31.00 Å, c = 45.00 Å, α = 90°, β = 90°, γ = 90°) and a second layer rotated by 90° around the *a*-axis was placed on top in order to arrange the mesogens in agreement with the X-ray results. Geometry optimization was performed with the force field "Universal" and the atom-based summation method.

*b) Model of the LC phase of ILC **1b** at 25 °C*

Nine ILCs **1b** have been placed side by side in a P1 unit cell with rectangular symmetry (a = 31.00 Å, b = 31.00 Å, c = 44.80 Å, α = 90°, β = 90°, γ = 90°) and a second layer rotated by 90° around the *a*-axis was placed on top in order to arrange the mesogens in agreement with the X-ray results.

*c) Model of the LC phase of ILC **2** at 25 °C*

Nine ILCs **2** have been placed side by side in a P1 unit cell with rectangular symmetry (a = 27.40 Å, b = 27.40 Å, c = 43.80 Å, α = 90°, β = 90°, γ = 90°) and a second layer rotated by 90° around the A-axis was placed on top in order to arrange the mesogens in agreement with the X-ray results. After the set-up of the unit cells, the geometry optimization was first performed

with the force field “Universal” using the atom-based summation method. Finally, the Ewald summation method was applied, until the non-covalent interactions (electrostatic and van der Waals interactions) were large and negative.

*b) Model of the LC phase of ILC **2** at –10 °C*

Nine ILCs **2** have been placed side by side in a P1 unit cell with rectangular symmetry (a = 23.623 Å, b = 23.623 Å, c = 80.00 Å, α = 90°, β = 90°, γ = 90°) and a second layer rotated by 90° around the a-axis was placed on top in order to arrange the mesogens in agreement with the X-ray results. After the set-up of the unit cells, the geometry optimization was first performed with the force field “Universal” using the atom-based summation method. Every 200 optimizations steps, the unit cell was reduced and the molecules displaced along the c-axis by 5 Å until the final unit cell with c = 60.30 Å was reached. Finally, the Ewald summation method was applied, until the non-covalent interactions (electrostatic and van der Waals interactions) were large and negative.

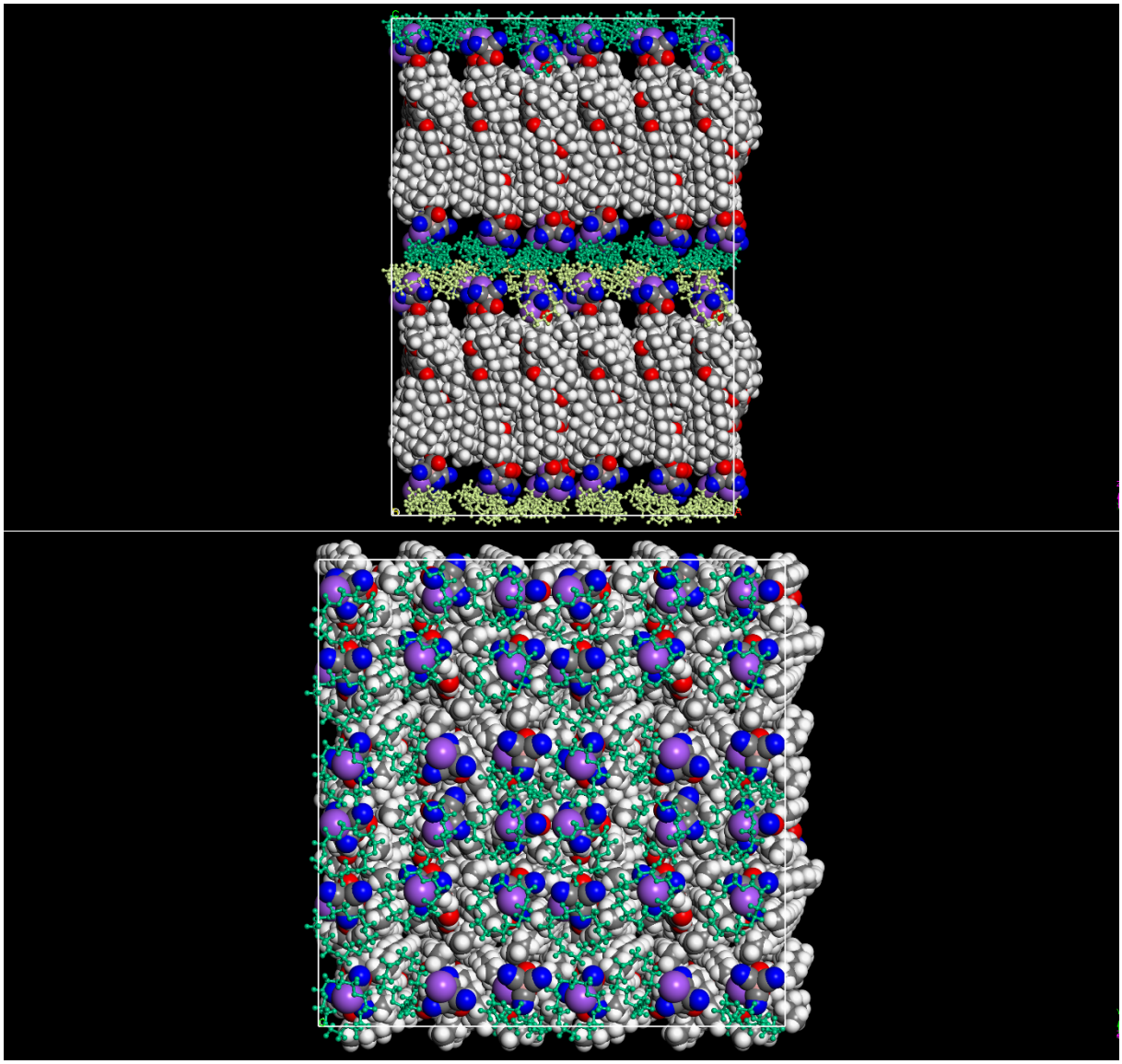

Figure S 24. LC phase model of ILC **1a** at 25 °C with 2x2x2 unit cells. Anions are shown as CPK models (C grey, H white, O red, N blue, B beige, Na light purple). Crown ethers are shown as ball and stick models. The crown ether layers are shown in dark resp. light green.

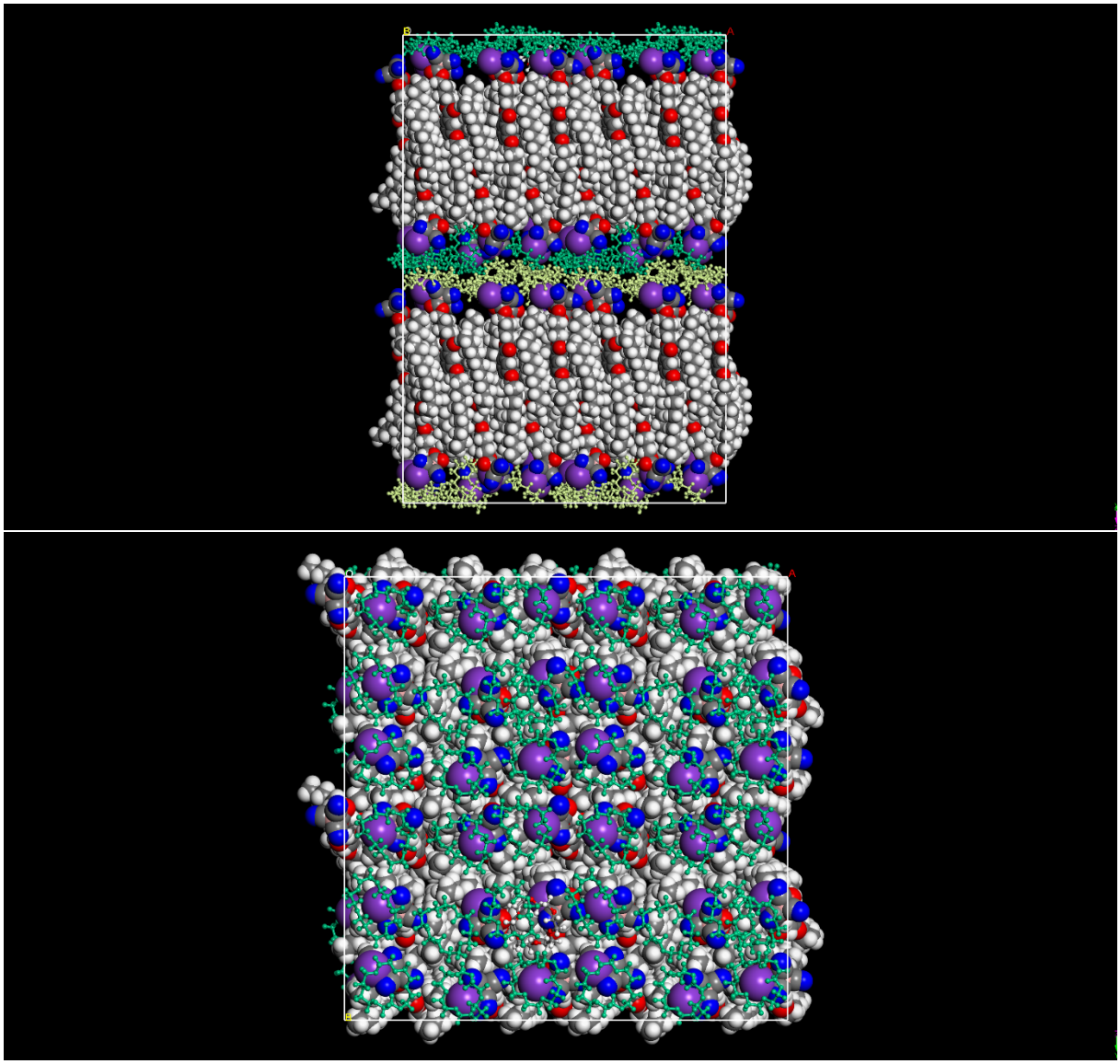

Figure S25. LC phase model of ILC **1b** at 25 °C with 2x2x2 unit cells. Anions and potassium are shown as CPK models (C grey, H white, O red, N blue, B beige, K purple). Crown ethers are shown as ball and stick models. The crown ether layers are shown in dark resp. light green.

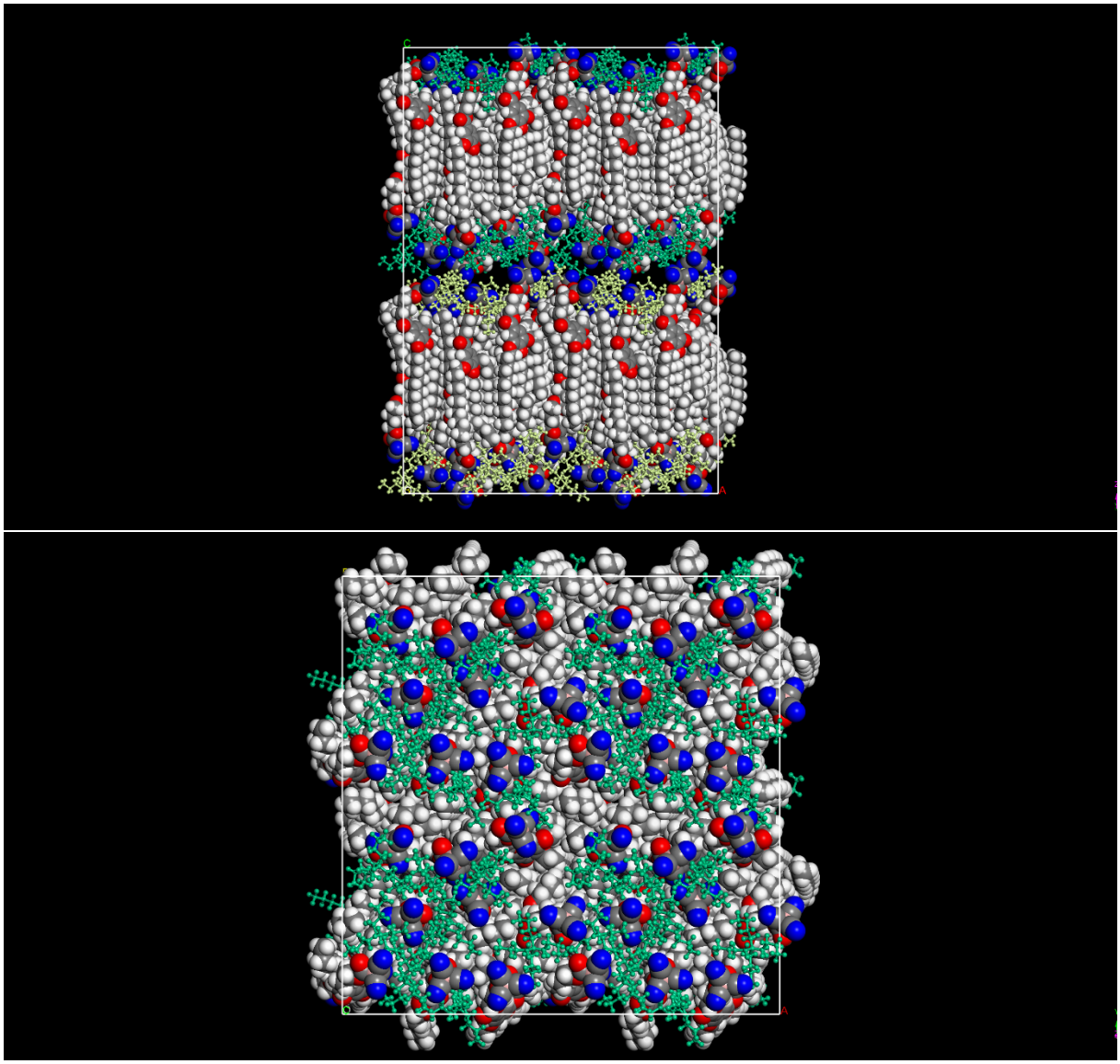

Figure S26. LC phase model of ILC **2** at 25 °C with 2x2x2 unit cells. Anions are shown as CPK models (C grey, H white, O red, N blue, B beige). Cations are shown as ball and stick models. The cation layers are shown in dark resp. light green.

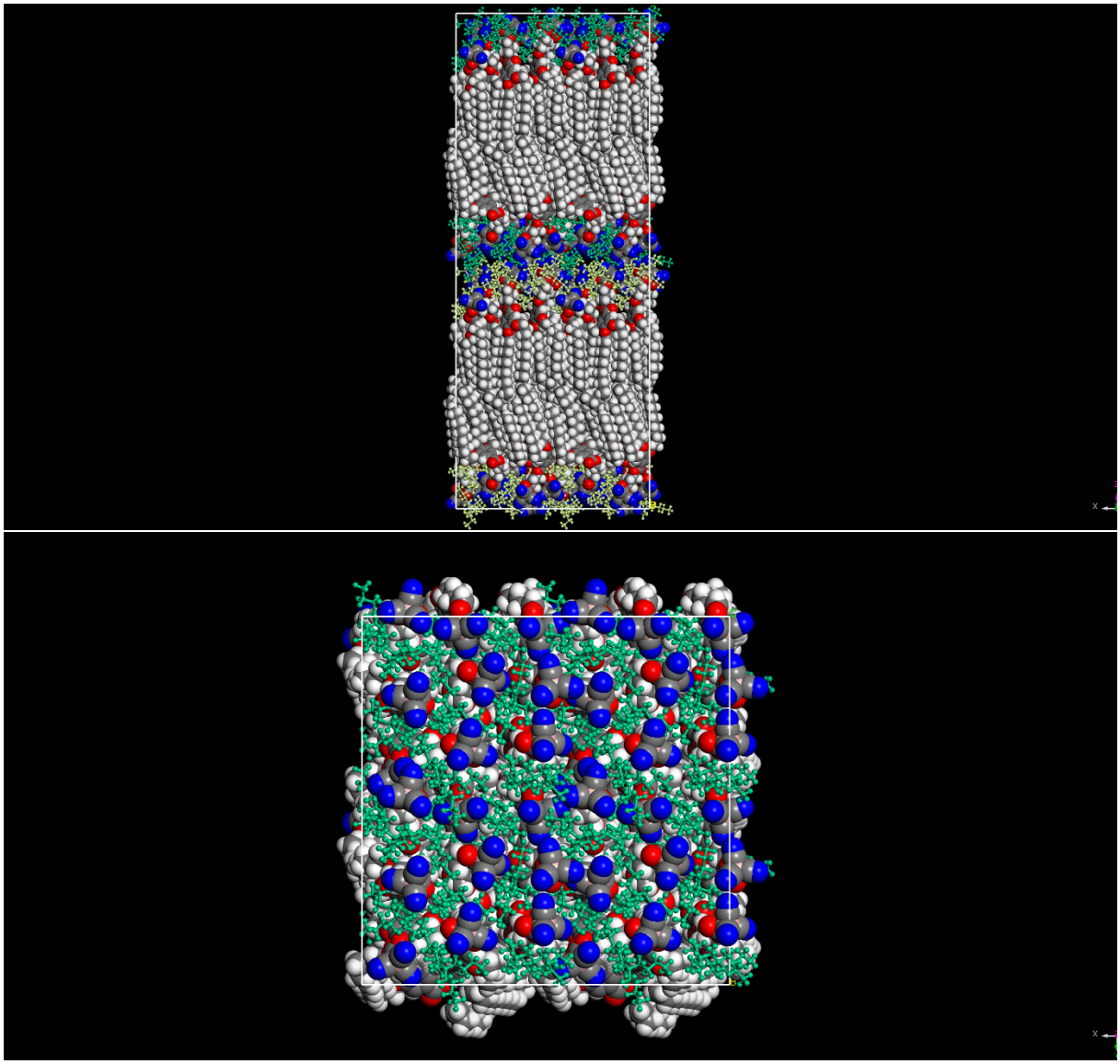

Figure S27. Phase model of ILC **2** at –10 °C with 2x2x2 unit cells. Anions are shown as CPK models (C grey, H white, O red, N blue, B beige). Cations are shown as ball and stick models. The cation layers are shown in dark resp. light green.

9) Electrochemical Impedance Spectroscopy

The ionic conductivity of the ILCs was determined via electrochemical impedance spectroscopy (EIS). Commercial Soda-lime glass LC cells (Instec, Inc.) with a homogeneous (model SG100A080uG180, 100 mm^2 ITO area, 100 Ω ITO resistance) resp. homeotropic alignment layer (model SG035A080uT180, 35 mm^2 ITO area, 25 Ω ITO resistance) were filled with the ILCs at 100 °C. Although with the conventional liquid crystal 4-cyano-4'-pentylbiphenyl (5CB), the cells showed the expected alignment (homogeneous and homeotropic for the respective alignment layer), both cell types resulted in a homogeneous alignment of the SmA phase of the ILCs with an multidomain structure (Figure S28). However,

by changing the thermal history for **1a** (see below part 1), the alignment became homeotropic. Therefore, the data presented is only that obtained with the cell model SG035A080uT180. An adhesive copper tape was used for electrical contact. The cells were placed in a climate chamber (Weiss Klimatechnik GmbH) and connected to a potentiostat (VMP-300, Bio-Logic SAS). The temperature program was chosen based on the onset transitions from the DSC data and thus was as follows (all values in °C): i) **1a** (homogenous) - 20, 30, 40, 50, 60, 65, 70, 75, 80, 85, 90, 85, 80, 75, 70, 65, 60, 50, 40, 30, 20, 10, 0; ii) **1a** (homeotropic) - part 1: 1 h temperature hold only, no EIS – 25, 95, -15, 20; part 2: temperature procedure with EIS as described below – 25, 30, 35, 40, 45, 50, 55, 60, 65, 70, 75, 80, 85, 90, 85, 80, 75, 70, 65, 60, 55, 50, 45, 40, 35, 30, 25, 20; iii) **1b** - 20, 30, 40, 50, 60, 70, 80, 90, 80, 90, 60, 90, 40, 90, 20, 90, 0; and iv) **2** - 20, 30, 40, 50, 60, 50, 40, 30, 20, 10, 0, 10, 20, 30, 40, 50, 60. At each temperature, an open circuit voltage (OCV) step was used to give the samples time to reach the desired temperature. Then, an EIS measurement was conducted in the frequency range of 7MHz to 100mHz with an amplitude of 10mV. After a further 5 min OCV step, the EIS measurement was repeated with the same parameters to check if the impedance deviated before the temperature was changed. The EIS data was transformed into permittivity data using the WinFit software (Novocontrol Technologies, Montabaur, Germany) and fit as described in references[S6,7] to determine the conductivity values.

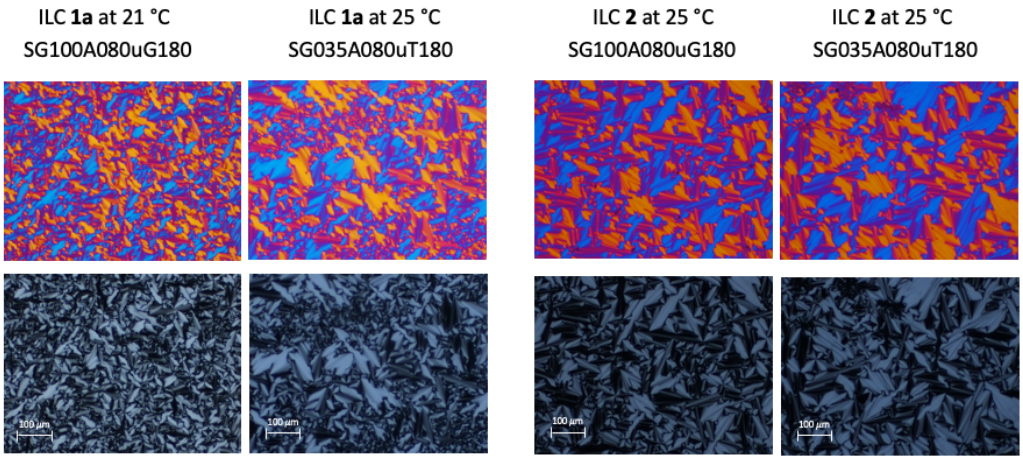

Figure 28. Textures in the liquid crystal cells for ILC **1a** and **2**. Top: Textures with a λ/2 compensator plate, highlighting the different orientations of the layers in the domains. Bottom: Textures without the λ/2 compensation plate.

Supplementary References

[S1] P. A. Heiney, *Datasqueeze 3.0.19*, **2004-2021**, http://www.datasqueezesoftware.com/.

[S2] E. Terazzi, S. Torelli, G. Bernardinelli, J.-P. Rivera, J.-M. Bénech, C. Bourgogne, B. Donnio, D. Guillon, D. Imbert, J.-C. G. Bünzli et al., *J. Am. Chem. Soc.* **2005**, *127*, 888–903.

[S3] Y.-J. Choi, D. Jung, S.-I. Lim, W.-J. Yoon, D.-Y. Kim, K.-U. Jeong, *ACS Appl. Mater. Interfaces* **2020**, *12*, 33239–33245.

[S4] V. Percec, D. Tomazos, J. Heck, H. Blackwell, G. Ungar, *J. Chem. Soc., Perkin Trans. 2* **1994**, 31–44.

[S5] S. Kavesh, J. M. Schultz, *J. Polym. Sci., Part A-2: Polym. Chem.* **1970**, *8*, 243–276.

[S6] V. Di Noto, G. A. Giffin, K. Vezzù, M. Piga, S. Lavina, "Broadband Dielectric Spectroscopy: A Powerful Tool for the Determination of Charge Transfer Mechanisms in Ion Conductors" in *Solid State Proton Conductors*: *Properties and Applications in Fuel Cells,* Knauth, Philippe; Di Vona, Maria Luisa, John Wiley & Sons, Ltd: Chichester, **2012**, 109–183.

[S7] G. A. Giffin, G. M. Haugen, S. J. Hamrock, V. Di Noto, *J. Am. Chem. Soc.* **2013**, *135*, 822–834.